Regeneration of Bipolar Cells in the Adult Zebrafish Retina

A Dissertation

Presented in Partial Fulfillment of the Requirements for the Degree

of Doctor of Philosophy

with a

Major in Neuroscience

in the

College of Graduate Studies University of Idaho

by

Timothy McGinn

Major Professor: Deborah Stenkamp, Ph.D.

Committee Members: Peter Fuerst, Ph.D., Onesmo Balemba, Ph.D., Lane Brown, Ph.D.

Department Administrator: James Nagler, Ph.D.

December 2016

Authorization to Submit Dissertation

The dissertation of Timothy McGinn, submitted for the degree of Doctor of Philosophy with a Major in Neuroscience titled, "Regeneration of Bipolar Cells in the Adult Zebrafish Retina" has been reviewed in final form. Permission, as indicated by the signatures and dates given below, is now granted to submit final copies to the College of Graduate Studies for approval.

Major Professor: _____ Date: _____
Deborah Stenkamp, Ph.D.

Committee Members: _____ Date: _____
Peter Fuerst, Ph.D.

_____ Date: _____
Onesmo Balemba, Ph.D.

_____ Date: _____
Lane Brown, Ph.D.

Department
Administrator: _____ Date: _____
James Nagler, Ph.D.

Acknowledgements

I would especially like to thank my advisor, Dr. Deborah Stenkamp for taking me in as a graduate student and being an excellent mentor over these last 7 years. Her guidance and support has helped me grow extraordinarily as a scientist.

I would like to thank my committee members, Dr. Peter Fuerst, Dr. Lane Brown, and Dr. Onesmo Balemba, who helped me see this project from start to finish.

I am extremely grateful for the assistance Ruth Frey gave me over the years and for all those times that she went out of her way to help me out. CJ Jenkins for doing much of the statistics required for Chapter 2. Matt Singer for helping out immensely with R, and with my experimental designs and analyses, both the successful and failed ones (too bad we couldn't get some of our great ideas work out and become complete studies). I would also like to thank Tyler Lankford, Amber Trost, Alessandra Minette, Dylan Leoni, Natalie Partington, and Audri Sedgwick of the Stenkamp lab. Ann Norton of the UI's Optical Imaging Core, and the great experience I gained working for her during my assistantship in the Optical Imaging Core. To Dan Fong of Nikon, for helping to train me on the spinning disk microscope and going above and beyond in order to help me get the best images possible. To Dr. Celeste Brown and Chloe Stenkamp-Strahm for assistance with statistics and data visualization. To Dr. Diana Mitchell for discussion and evaluation of earlier versions of Chapter 2 and Chapter 3. As well as general help in the lab and with manuscript writing. My fellow graduate students in the Stenkamp lab: Susov Dhakal, Sun Chi, and Rob Mackin.

Dedication

This dissertation is dedicated to my parents, who have been very supportive
and encouraged my passion for science over the years.

Abstract

Adult zebrafish are capable of generating new neurons in the central nervous system, including the retina. Results from previous studies have suggested that some, if not all, of these newly generated retinal neurons are functional and reform functional circuitry. The complexity of this circuitry and the ability of these newly formed neurons to recapitulate circuitry formed during development has not been studied. These previous studies also did not measure the morphology and types of connections made by these newly formed neurons and did not examine adult retinas. The studies of this dissertation measured the morphological and bipolar cell to photoreceptor connectivity patterns of bipolar cells that expressed yellow fluorescent protein driven by the nyctalopin promoter or expressed PKCα. We hypothesized that these bipolar cells would restore the sizes of their dendritic fields and restore connections with SWS2 (blue), RH2 (green), and LWS (red) cones over a 60 day time-course (when visually-mediated reflexes are regained).

I selectively lesioned the neurons of the inner retina, by using the neurotoxin ouabain. Results from these studies found that retinal bipolar cells are present at 13 days post injection (DPI), (the first post-regeneration time point selected); however, these bipolar are morphologically distinct from those in an undamaged retina. These cells regain certain morphological characteristics by 17 DPI, but have reduced dendritic spreads at both 17 DPI and 21 DPI.

The dendritic spread as well as all other measurements taken, found that these types of bipolar cells at 60 DPI were no different than the control neurons. Previous studies that tested behavior also found that certain sight related behaviors returned by 60 DPI. Taken together, morphological measurements from studies presented in this dissertation and behavioral measurements from previous studies suggests that these newly generated neurons are accurate at rewiring and reintegrating themselves into functional circuits.

Table of Contents

List of Figures

List of Tables

CHAPTER 1: Introduction

Zebrafish (*Danio rerio*) have the ability to rapidly regenerate functional neurons in extensively damaged neuronal tissue, an ability that humans and mammals do not have (Sherpa, et al., 2008) (Bernardos, Barthel, Meyers, & Raymond, 2007) and (Thummel, et al., 2010). The mechanisms behind this ability have yet to be discovered and understood in a way that could be fully applicable to humans. The retina function and structure is conserved between zebrafish and humans. Both species have photoreceptors, bipolar cells, ganglion cells, amacrine, horizontal and Müller glia cells. This means that the mechanisms behind retinal regeneration, once understood, may be induced in humans and allow for rapid recovery after traumatic retinal injury and as part of treatments for retinal diseases. Mice are another commonly used laboratory animal model and are often used to study retinal diseases (Pennesi, Neuringer, & Courtney, 2012) but zebrafish have an additional advantage beyond their capacity for retinal regeneration. That is because, unlike mice, zebrafish rely primarily on cone photoreceptors for vision, just as humans do.

Understanding the anatomy and physiology of a healthy retina is necessary in order to understand the etiology and treatment of retinal diseases. Age related macular degeneration (AMD) results in photoreceptor loss, causing vision loss that often leads to blindness (Curcio, Medeiros, & Millican, 1996). Glaucoma is a group of conditions that also leads to blindness due to the loss of retinal ganglion cells and degeneration of the optic nerve. Quigley and Broman (2006), estimate that glaucoma is the second leading cause of blindness worldwide.

Retinas of humans respond to retinal degeneration and tissue loss due to trauma by reactive gliosis (Sethi, et al., 2005). In goldfish and zebrafish these Müller glia participate in neurogenesis (Wu, et al., 2001) (Nagashima, Barthel, & Raymond, 2013). Since mice and humans have the same retinal cells types, homologous proteins, and homologous genes, it is possible that small molecules, proteins, or gene therapy could induce human Müller glia to undergo neurogenesis instead of gliosis, by altering the expression of a few key genes.

There is are broad area of research that is discovering these molecular mechanisms of regeneration. Much of the current research is focused on uncovering how retinal Müller glial cells are able to dedifferentiate, divide, and create new neurons. (Lenkowski, et al., 2013) (Nagashima, Barthel, & Raymond, 2013) (Conner, Ackerman, Lahne, Hobgood, & Hyde, 2014)

In a light damage model, Bernardos, Barthel, Meyers, & Raymond (2007) found that Müller glia are the retinal stem cells that produce cones. They found that by 3 and 4 days after light lesioning Müller glia were rapidly dividing, expressed Pax6, mostly located in the inner nuclear layer (INL), and mostly absent from the outer nuclear layer (ONL) at 2 and 3 DPI. At 4 and 5 days post lesioning they found that these Müller glia cells had migrated to the ONL and started to expresses the protein Crx, which is normally only found in photoreceptors and the outer half of the INL. They also found that Müller glia are the progenitor cells for the rods that are generated in the adult fish. This suggests that many of the molecular and cellular mechanisms that allow teleost to continue to produce rods may also be responsible for regeneration.

This mechanism of regeneration may also not be limited to Müller glia and neurons of the retina. In addition to producing new neurons in the retina, the brain of the adult zebrafish is also capable of producing neurons. (Kroehne, Freudenreich, Hans, Kaslin, & Brand, 2011) found that the neuronal architecture of the brain was restored following a traumatic stab lesion. They also found that radial glial cells that expresses the protein her4.1, are the neuronal progenitor cells and migrate from the ventricular zone to the lesion site. These newly generated neurons appeared to be permanently integrated into the brain and appeared to have several characters of functional neurons. This is important because it shows that circuit restoration is possible across the entire CNS.

Evidence strongly supports that neuronal cells and overall function of the teleost retina are restored across several different models of damage and regeneration. Studies in goldfish and sunfish found that electroretinogram (ERG) function is restored and the dorsal light reflex (DLR) returns to normal (Mensinger & Powers, 1999) (Mensinger & Powers, 2007). Sherpa, et al., (2008) found similar

results in zebrafish, where they demonstrated that the escape response returns to normal by 98 days after the complete destruction of neuronal retinal cells. A study that removed a piece of dorsotemporal retina in adult goldfish found that new retinal ganglion cells are generated, and these newly generated ganglion cells have dendrites that are as morphologically complex as existing ganglion cells, and these newly formed ganglion cells regain certain physiological properties (Cameron, Vafai, & White, 1999). That same study also found examples of anomalously long dendrites, in a few of the RGCs as well as bundles of RGCs that only appeared in regenerated portions of the retina. Other studies that selectively killed only the ganglion cell layer and inner nuclear layer, found that the regenerated retina was still disorganized, but not to the extent of a completely destroyed then regenerated retina (Fimbel, Montgomery, Burket, & Hyde, 2007) and (Sherpa, et al., 2008) (Sherpa, et al., 2014). Sherpa, et al., (2014) also demonstrated the restoration of visual function in fish with selectively lesioned retinas by using the DLR, as well as a place preference assay.

These previous studies demonstrated the ability of the retina to become functional and regain basic functional connections to brain. These previous studies only looked at complex morphology of retinal ganglion cells. This means there is a significant knowledge gap, in that the complexity of these restored circuits are not known and morphology and connectivity pattern of the bipolar cells that connect the photoreceptors to ganglion cells has not yet been documented. There is also a significant knowledge gap in the manner in which these bipolar cells regenerate. Do they all come back in synchronized manner, as they do during development or do they provide a different type of plasticity that means growth and refinement?

Connaughton, Graham, & Nelson (2004) describe 17 different types of bipolar cells based upon their morphology and axonal stratification. They also divided up those 17 different types of bipolar cells up into 3 different categories based upon function and axonal stratification (ON, OFF, Mixed ON/OFF). (Li, Tsujimura, Kawamura, & Dowling (2012) found that there are 19 different categories of bipolar cells in zebrafish based upon their connectivity patterns with photoreceptors.

Transgenic zebrafish that express yellow fluorescence protein (YFP) in BP cells that endogenously produce nyctalopin allow for entire bipolar cells to be imaged and measured by confocal microscopy. In this current study we measured dendritic and axonal complexity, as well as, the connectivity pattern of nyctalopin expressing retinal bipolar cells, in the regenerated retina. The data from this study provide very strong vidence that retinal bipolar cells are restored and integrate to become part of a reformed functional retina.

References

Bernardos, R. L., Barthel, L. K., Meyers, J. R., & Raymond, P. A. (2007, June 27). *Late-Stage Neuronal Progenitors in the Retina Are Radial Muller Glia That Function as Retinal Stem Cells.* The Journal of Neuroscience, 27(1), 7028-7040.

Cameron, D. A., Vafai, H., & White, J. A. (1999, March). *Analysis of dendritic arbors of native and regenerated cells in the goldfish retina.* Visual Neuroscience, 16(2), 253-261.

Connaughton, V. P., Graham, D., & Nelson, R. (2004, September 27). *Identification and Morphological Classification of Horizontal, Bipolar, and Amacrine Cells within the Zebrafish Retina.* The Journal of Comparative Neurology, 477(4), 371–385. doi:10.1002/cne.20261

Conner, C., Ackerman, K. M., Lahne, M., Hobgood, J. S., & Hyde, D. R. (2014, October 22). *Repressing Notch Signaling and Expressing TNFα Are Sufficient to Mimic Retinal Regeneration by Inducing Müller Glial Proliferation to Generate Committed Progenitor Cells.* Journal of Neuroscience, 34(43), 14403-14419.

Curcio, C. A., Medeiros, N. E., & Millican, C. L. (1996). *Photoreceptor Loss in Age-Related Macular Degeneration.* Investigative Ophthalmology & Visual Science, 37(7), 1236-1249.

Ferreira, T. A., Blackman, A. V., Oyrer, J., Jayabal, S., Chung, A. J., Watt, A. J., . . . van Meyel, D. J. (2014, October 11). *Neuronal Morphometry Directly from Bitmap Images.* Nature Methods, 11(10), 982-984.

Fimbel, S. M., Montgomery, J. E., Burket, C. T., & Hyde, D. R. (2007, February 14). *Regeneration of Inner Retinal Neurons after Intravitreal Injection of Ouabain in Zebrafish.* The Journal of Neuroscience, 27(7), 1712-1724.

Kroehne, V., Freudenreich, D., Hans, S., Kaslin, J., & Brand, M. (2011, October 17). *Regeneration of the adult zebrafish brain from neurogenic radial glia-type progenitors.* Development, 138(22), 4831-4841.

Lenkowski, J. R., Qin, Z., Sifuentes, C. J., Thummel, R., Soto, C. M., & Raymond, P. A. (2013, August 5*). Retinal regeneration in adult zebrafish requires regulation of TGFβ signaling.* Glia, 61(10), 1687-1697.

Li, Y. N., Tsujimura, T., Kawamura, S., & Dowling, J. E. (2012, November 1). *Bipolar Cell–Photoreceptor Connectivity in the Zebrafish (Danio rerio) Retina.* The Journal of Comparative Neurology, 520(16), 3786–3802.

Mensinger, A. F., & Powers, M. K. (1999). *Visual function in regenerating teleost retina following cytotoxic lesioning.* Visual Neuroscience, 16, 241-251.

Mensinger, A. F., & Powers, M. K. (2007). *Visual function in regenerating teleost retina following surgical lesioning.* Visual Neuroscience, 24, 299-307.

Nagashima, M., Barthel, L. K., & Raymond, P. A. (2013, October). *A self-renewing division of zebrafish Müller glial cells generates neuronal progenitors that require N-cadherin to regenerate retinal neurons.* Development, 140(22), 4510-4521.

Pennesi, M. E., Neuringer, M., & Courtney, R. J. (2012, August). *Animal models of age related macular degeneration (review).* Molecular Aspects of Medicine, 33(4), 487-509.

Quigley, H. A., & Broman, A. T. (2006, March). *The number of people with glaucoma worldwide in 2010 and 2020.* British journal of ophthalmology, 90(3), 262-267.

Raymond, P. A., Reifler, M. J., & Rivlin, P. K. (1988, July). *Regeneration of goldfish retina: rod precursors are a likely source of regenerated cells.* Journal of Neurobiology, 19(5), 431-463.

Ristanovic, D., Milosevic, N., & Stulic, V. (2006, December 15). *Application of modified Sholl analysis to neuronal dendritic arborization of the cat spinal cord.* Journal of Neuroscience Methods, 158(2), 212-218.

Schroeter, E. H., Wong, R. O., & Gregg, R. G. (2006, September-October). *In vivo development of retinal ON-bipolar cell axonal terminals visualized in nyx::MYFP transgenic zebrafish.* Visual Neuroscience, 23(5), 833-843.

Sethi, C. S., Lewis, G. P., Fisher, S. K., Leitner, W. P., Mann, D. L., Luthert, P. J., & Charteris, D. G. (2005, January*). Glial remodeling and neural plasticity in human retinal detachment with proliferative vitreoretinopathy.* Invest. Ophthalmol. Vis. Sci., 46(1), 329-342.

Sherpa, T., Fimbel, S. M., Mallory, D. E., Maaswinkel, H., Spritzer, S. D., Sand, J. A., . . . Stenkamp, D. L. (2008, Feburary 1). *Ganglion Cell Regeneration Following Whole-Retina Destruction in Zebrafish.* Developmental Neurobiology, 68(2), 166-181.

Sherpa, T., Lankford, T., McGinn, T. E., Hunter, S. S., Frey, R. A., Ryan, M., . . . Stenkamp, D. L. (2014, September 1). *Retinal Regeneration is Facilitated by the Presence of Surviving Neurons.* Developmental Neurobiology, 74(9), 851-876.

Thummel, R., Enright, J. M., Kassen, S. C., Montgomery, J. E., Bailey, T. J., & Hyde, D. R. (2010, Feburary 10). *Pax6a and Pax6b are required at different points in neuronal progenitor cell proliferation during zebrafish photoreceptor regeneration.* Experimental Eye Research(90), 572-582.

Wu, D. M., Schneiderman, T., Burgett, J., Gokhale, P., Barthel, L., & Raymond, P. A. (2001, August). *Cones regenerate from retinal stem cells sequestered in the inner nuclear layer of adult goldfish retina.* Investigative Ophthalmology & Visual Science, 42(9), 2115-2124.

CHAPTER 2: Restoration of Dendritic Complexity, Connectivity, and Diversity of Regenerated Retinal Bipolar Neurons in Adult Zebrafish

(Submitted to Journal of Neuroscience by Timothy E. McGinn, Natalie Partington, Dylan Leoni, Christina E. Jenkins, and Deborah L. Stenkamp*)

Abstract

Adult zebrafish (*Danio rerio*) have the ability to regenerate retinal neurons that have been lost due to mechanical, chemical, or light damage. In the case of chemical damage, there is evidence that visually-mediated behaviors are restored following regeneration, consistent with the recovery of retinal function. However, the extent to which regenerated retinal neurons attain appropriate morphologies and circuitry after such tissue-disrupting lesions has not been investigated. We examined dendritic and axonal morphologies, connectivity patterns, and the diversities of each, for a subpopulation of retinal bipolar neurons that regenerated after the destruction of the inner retina using the neurotoxin ouabain. We used a combination of cell-selective markers, confocal microscopy, and morphometrics including Sholl analysis to compare regenerated retinal neurons to those in undamaged retinas. We found that bipolar cell dendritic spread, dendritic tree morphology, as well as cone to bipolar cell connectivity patterns were restored in regenerated retinas, suggesting that regenerated bipolar neurons recover accurate input pathways from surviving cone photoreceptors. Morphological measurements of bipolar axons found that numbers and types of stratifications were also restored; however, the thickness of the inner plexiform layer, and one measure of axon branching were each slightly reduced following regeneration, suggesting some minor differences in the recovery of output pathways to downstream partners that have also regenerated. These results support the hypothesis that regenerated neurons of the adult zebrafish retina are capable of restoring complex morphology and circuitry, suggesting that complex visual functions may also be restored.

Significance Statement

Adult zebrafish are capable of generating new retinal neurons after a tissue-disrupting lesion. Existing research does not address whether regenerated neurons of adults are successful at reconnecting with surrounding neurons and establishing complex morphologies. We report that, after a chemical lesion that ablates inner retinal neurons, regenerated retinal bipolar cells reconnect to undamaged cone photoreceptors with correct wiring patterns. Using Sholl analysis we found that regenerated retinal bipolar cells have complex morphologies similar to those within undamaged retina. This new understanding of neural connectivity and morphological complexity suggests that complex functional processing is possible within regenerated adult retina, and offers a system for future study of mechanisms involved in neurite growth and synapse formation during regeneration of adult retina.

Introduction

The human retina cannot regenerate neurons that are lost due to retinal disease or trauma, while retinas of teleost fish have this capacity (Stenkamp, 2007). Our understanding of mechanisms underlying teleost retinal regeneration has expanded significantly in the last decade, largely due to the identification of Müller glia as the stem cell source of regenerated neurons (Fausett and Goldman, 2006; Bernardos et al., 2007), and to the use of a versatile animal model – the zebrafish – in addition to previous models for retinal regeneration (Stenkamp, 2007). The potential within mammalian retinas to activate mechanisms that can initiate the Müller glial response has been documented (Karl et al., 2008), catalyzing efforts toward developing regenerative therapies for human retinal disorders (Ahmad et al., 2011).

Previously, we documented the restoration of visual function in adult zebrafish subjected to chemical damage of the retina and a recovery period, measuring simple reflexes and place-preference behaviors (Sherpa et al., 2008; Sherpa et al., 2014). These results indicated that at least some functional synaptic connections are made within regenerated retina. However, a series of studies utilizing diverse modes of

retinal damage has shown that the regenerated adult fish retina displays patterning abnormalities in lamination (Sherpa et al., 2014), and in two-dimensional organization of specific neuronal classes (Hitchcock et al., 1992; Stenkamp et al., 2001). The regenerating adult zebrafish retina also generates supernumerary neurons (Sherpa et al., 2008; Sherpa et al., 2014; Powell et al., 2016), including those that were not lost to damage (Powell et al., 2016). Together these observations suggest that regenerated retinal neurons may be capable of accurate re-wiring even in a disrupted microenvironment, and despite abnormal cellular patterns. Previous work in regenerated adult goldfish retina showed that individual synaptic terminals of regenerated neurons in OPL and IPL were normal at an ultrastructural level (Hitchcock and Cirenza, 1994), and that regenerated neurons could functionally integrate with undamaged neurons in the lateral dimension via gap junctions (Hitchcock, 1997). However, the degree to which regenerated retinal neurons in adult fish establish a normal retinal connectome – to the correct type and number of synaptic partners – and whether regenerated neurons attain normal morphologies consistent with function, remains unestablished.

Recently, D'Orazi et al. (D'Orazi et al., 2016) discovered that selected subpopulations of regenerated retinal bipolar neurons of the growing larval zebrafish retina established essentially normal morphologies and regain connectivity patterns with their undamaged synaptic partners, displaying some minor errors. Therefore, it remains unclear whether regenerated retinal neurons can also restore appropriate morphologies and connectivity patterns with synaptic partners that have also regenerated, whether they can do so within a disturbed environment of more profound retinal damage, and whether either of these can take place in adult animals.

In the present study we focus upon a morphologically diverse subpopulation of retinal bipolar neurons that is regenerated after a chemical lesion that destroys all inner retinal neurons but spares photoreceptors and Müller glia (Fimbel et al., 2007; Nagashima et al., 2013; Sherpa et al., 2014). Regenerating bipolar neurons were therefore challenged to elaborate their dendritic and axonal processes, and to find presynaptic partners that were undamaged (cone photoreceptors), as well as postsynaptic partners that were themselves regenerating (amacrine and ganglion

cells) (Fimbel et al., 2007; Nagashima et al., 2013; Sherpa et al., 2014). Through detailed morphometric analyses of dendritic and axonal attributes, as well as analyses of photoreceptor connectome and axon stratification patterns, we conclude that regenerated retinal bipolar neurons show morphologies and connectomes, and diversities of each of these, which are broadly consistent with the restoration of complex retinal functions.

Materials and Methods

Animals and retinal lesioning.

All zebrafish were treated in accordance to protocols approved by The University of Idaho Institutional Animal Care and Use Committee and were raised and maintained according to (Westerfield, 2007) on a 14:10 hour light:dark cycle in monitored, recirculating system water. Zebrafish transgenic strains used in this study were *nyx::mYFP* (two transgenes likely co-integrated: nyctalopin (nyx) promoter driving gal4 and the UAS enhancer element driving MYFP) (Schroeter et al., 2006), with YFP expressed in retinal bipolar (BP) neurons; SWS2:mCherry (Takechi et al., 2008), with mCherry expressed in blue-sensitive cones; and SWS1:GFP (Takechi et al., 2003), with GFP expressed in UV-sensitive cones.

The retinas of adult fish (6-16 months) were chemically lesioned by intravitreal injection of ouabain to selectively destroy inner retinal neurons while sparing photoreceptors and Müller glia (Wolburg and Maier, 1979; Fimbel et al., 2007; Nagashima et al., 2013; Sherpa et al., 2014). Briefly, fish were anaesthetized by tricaine and an incision was made across the cornea and iris with a sapphire knife. Using a Hamilton syringe (26s) 0.4 µL - 0.6 µL of 70 µM ouabain in saline was injected into the vitreal chamber of one eye, resulting in an estimated intraocular concentration of 2 µM. The contralateral eyes of lesioned fish served as uninjected, undamaged controls. Loss of bipolar (BP) neurons and survival of cones was verified in sectioned retinas obtained from parallel experiments at three days post-injury (3DPI) (Fig. 2.1), and by viewing retinas of live, anaesthetized fish with epifluorescence stereomicroscopy (Nikon SMZ 1500), also at 3DPI.

Tissue processing and immunocytochemistry.

Fish were euthanized with tricaine and eyes enucleated. To obtain retinal cryosections, whole eyes were fixed in phosphate-buffered (pH=7.4), 4% paraformaldehyde containing 5% sucrose for one hour. Eyes were then washed, cryoprotected, embedded, and then frozen in a 1:2 solution of Tissue-Tek OCT embedding medium (Sakura Finetek) and phosphate-buffered, 20% sucrose (Sherpa et al., 2008; Sherpa et al., 2011; Sherpa et al., 2014). Eyes were cryosectioned at 5 μm or 20 μm.

To obtain whole, flat-mounted retinas, enucleated eyes were perforated through the cornea with a 27-gauge needle and the hole expanded with dissecting scissors. The lens was removed through the incision and then the sclera and RPE were peeled away with forceps to free the retina. Retinas were rinsed in cold HEPES or phosphate-buffered saline (PBS) and 4 radial incisions were made to facilitate flattening the retina. Retinas were then fixed for 1 hour at room temperature in phosphate-buffered 4% paraformaldehyde containing 5% sucrose.

For immunohistochemistry, 5 μm and 20 μm sectioned retinas were rinsed with phosphate buffered saline with 0.5% triton (PBST) and then blocked for 1 hour at room temperate with 20% normal goat serum and 0.1% sodium azide, diluted in PBST. Sections were stained with primary antibodies diluted in antibody dilution buffer (PBST, 1% normal goat serum, and 0.1% sodium azide). Sections were incubated overnight at 4°C, washed 3 times with PBST, then incubated with secondary antibodies diluted in antibody dilution buffer and 4.25 μM DAPI overnight at 4°C. Whole retinas were stained with primary antibodies in antibody dilution buffer for 1-2 weeks at 4°C, washed 3 times with PBST, then incubated with secondary antibodies diluted in antibody dilution buffer and 4.28 μM DAPI at 4°C for another week. Slides or retinas were washed 3x30 minutes in PBS prior to mounting.

Primary antibodies used in this study (source; dilution) were as follows. ZPR1 is a mouse monoclonal that labels cone arrestin-a, staining both members of the red- and green-wavelength sensitive double cone pair (Renninger et al., 2011) (ZIRC; 1:200). Anti-protein kinase Cα (PKCα) is a rabbit polyclonal antibody originally produced from the C-terminus of human PKCα, mapped at amino acids 372-672.

PKCα labels a subpopulation of BP neurons (Suzuki and Kaneko, 1990) (Santa Cruz Biotechnology; SC-10800 1:200). Anti-synaptic vesicle 2 (SV2) is a mouse monoclonal antibody that labels synaptic terminals (Yazulla and Studholme, 2001) (Developmental Studies Hybridoma Bank; 1:2000). Secondary antibodies used in this study are donkey anti-mouse Dylight 649 (Jackson Labs; 1:200), and donkey anti-rabbit Cy3 (Jackson Labs; 1:200).

Imaging, analysis, and statistics.

Sectioned, stained retinas were mounted in Fluoromount-G (SouthernBiotech), or Vectashield Hardset (Vector Laboratories) with number 1 coverslips (Fisher Scientific). Some sections were imaged using a 20x 0.75NA air objective or a 60x, 1.42NA oil immersion objective on an Olympus FV1000 confocal microscope. Another set of sections was imaged with an Andor Zyla 5.5 sCMOS camera connected to a Nikon Ti inverted microscope with a Yokogawa spinning disk using a 20x 0.75NA air objective, a 60x 1.40NA, or 100x 1.45NA oil immersion objective.

Whole retinas were flattened and mounted on microscope slides in Fluoromount-G or Vectashield Hardset with number 1 coverslips with GCL facing the coverslip. Electrical tape was used as a spacer between the coverslip and slide. Whole, flat-mounted retinas were imaged with the Andor/Nikon system described above using a 20x air 0.75NA objective or a 60x 1.2NA water immersion objective, with Immersol W 2010 (Zeiss). Using the 60x lens, multiple image stacks were collected using 0.3 μm z-steps through the entire thickness of the retina. Each stack was 114.62 μm wide by 164.88 μm high (1028x1522 pixels) resulting in a scale of 9.23 pixels/μm. Most image stacks were collected from regions outside of the larval remnant surrounding the optic nerve head (Allison et al., 2011), and avoiding the most peripheral regions.

Image stacks were analyzed in Fiji software (ver 1.51d) (Fiji, RRID:SCR_002285) (Schindelin et al., 2012). Images were gathered from multiple locations across the retina. Generally, most confocal image stacks were taken near the central retina as well as several adjacent areas. Additional confocal image stacks were taken in the mid-periphery where *nyx::mYFP*+ cells were clearly isolated. Selected *nyx::mYFP*+ cells were traced using the Simple Neurite Tracer (SNT) plugin

(Longair et al., 2011). While some sampled *nyx::mYFP*+ cells were clearly isolated, others had near or overlapping neighbors. These neurons were included in this study to ensure that multiple types and locations of *nyx::mYFP*+ cells were sampled and traced. Dendritic spread was measured using the ellipse method, in which an ellipse was drawn around the perimeter of the dendritic tips and the area of the ellipse recorded (Li et al., 2012), or using a convex polygon, in which a polygon was drawn around the outermost tips of the dendrites and the area was recorded (Kraft et al., 2006).

Sholl analysis was carried out on traced bipolar cell dendrites and axons. Using the Sholl analysis option in SNT, data for each dendrite and axon were separately exported as column separated value files (.CSV) that contained the number of intersections at each radial distance from the center. These .CSV files were batch analyzed using the Sholl Analysis Plugin (ver 3.6.2) packaged with Fiji (Ferreira et al., 2014). For dendrites, the point at which the primary dendrite branched to generate the dendritic network was considered the center point. The center point used for the axons was at the furthest stratification point from the soma and where the axon initially branched.

In order to identify connections of cones to *nyx::mYFP* BPs, original .ND2 raw images were imported into Fiji (Schindelin et al., 2012). Dendrites of *nyx::mYFP* BPs were each traced separately in SNT. Traced dendrites were filled in using the "fill" option and independent stacks for each dendrite were generated. These stacks were remerged into the original stack as separate channels. Only the channels that included ZPR1+ cones, SWS2:mCherry (blue-sensitive) cones, and the traced BP neuron were viewable. A partial Z-projection was generated such that the projected image only contained the synaptic pedicles of the cones and the dendritic field of the BP cell being analyzed. Using the Region of Interest (ROI) tool in FIJI, the synaptic pedicles of the SWS2:mCherry cones and the ZPR1+ cones were outlined as separate colors. In many cases, the identity of ZPR1+ pedicles as belonging to an RH2 vs. LWS (green- vs. red-sensitive) cone could be determined from the image because this marker more strongly labels red-sensitive cones. In addition, cone identities could be established based upon their location within the cone mosaic of

the zebrafish retina (Allison et al., 2011; Li et al., 2012). Each dendritic tip that connected with an identified cone pedicle was recorded, as well as the total number of dendritic tips for each BP cell analyzed.

Using Fiji, individually traced neurons were cropped and then resliced using the "Stacks Reslice [/]" tool. This generated images with radial views of the retina such that the IPL could be subdivided into 6 equivalent strata (Connaughton et al., 2004). Axon stratification patterns of individual BP cells were determined by recording the stratum or strata that contained axon terminals.

The thickness of the IPL, and of the overall length of the BPs, were measured by using the straight line tool in Fiji, using PKCα-stained cryosections. For IPL thickness the line was drawn from the innermost portion of the DAPI+ or SV2- portion of the INL, to the most distal tips of PKCα+ axons in the deepest IPL stratum. For overall bipolar cell length, the line was drawn from the most distal point of the primary dendrites of PKCα+ BP neurons to the deepest tips of the primary axons. Each measurement was taken from three different locations of one radially-oriented section, and averaged, for each of 3 eyes per condition.

Densities of *nyx::mYFP* BP neurons were measured from *nyx::mYFP* retinal flat mounts (n=4 per condition for this analysis), by imaging the entire retina and stitching with Nikon Elements software. Retinal perimeters were traced in FIJI to obtain retinal areas, and YFP+ profiles > 5 μm diameter were counted using the analyze particles tool. BP neuronal densities were also measured from PKCα-stained cryosections (n=3 per condition for this analysis), by counting PKCα+ cell bodies across radial sections imaged at 20x and sampled between the larval remnant and the extreme periphery. In order to calculate BP density, these counts were divided by an area consisting of the linear distance of the section multiplied by section thickness.

Data were imported into R Studio (ver 0.99.491) (R Project for Statistical Computing, RRID:SCR_001905) using R (ver 3.2.2) (CRAN, RRID:SCR_003005) for statistical analysis. Sampling depth for each parameter and characteristic ranged from 11-30 individual neurons per condition, with neurons sampled from 10 different undamaged eyes and 6 different eyes collected at 60 DPI. Welch's 2-sample t-tests,

paired t-tests, and Kruskal-Wallis tests were used for parametric and most non-parametric data, respectively. A generalized linear model with a Poisson distribution was applied for analysis of connectivity patterns and axon stratification patterns. A Fisher's exact test was used to analyze proportions of ON vs. Mixed ON/OFF type BPs.

In order to determine if our measurements were differentially correlated in control vs. regenerated retinas, we performed a linear regression within each eye for each combination of measurements of interest. The resultant coefficients for correlation (slopes of the linear regressions for each eye) were the units for comparison between regenerated and control samples, and were analyzed by Kruskal-Wallis rank sum test.

Results

Intravitreal injection of 2 µM ouabain destroys retinal bipolar neurons while preserving cone photoreceptors.

To damage the adult zebrafish retina and create a disrupted environment to challenge regenerated neurons to establish appropriate morphologies and connectomes, we used intravitreal injection of 2 µM ouabain. We and others have demonstrated that this lesioning strategy destroys retinal ganglion cells, amacrine cells, bipolar cells, and all but a very small number of horizontal cells, while sparing photoreceptors and Müller glia (Fimbel et al., 2007; Nagashima et al., 2013; Sherpa et al., 2014). We again confirmed that 2 µM ouabain destroyed retinal bipolar (BP) neurons by observing BP populations that stain with antibodies targeting PKCα, and those expressing an mYFP reporter driven by the nyctalopin promoter *nyx::mYFP* (Bahadori et al., 2006; Schroeter et al., 2006). The *nyx::mYFP+* BPs constitute a subset of the PKCα+ BPs, likely at least in part due to mosaic silencing of the UAS promoter for mYFP (Schroeter et al., 2006). In control retinas, these markers identified neurons with cell bodies in the middle to outer half of the inner nuclear layer (INL) (Fig. 2.1A,D), and with axon terminals that stratified either in the inner half of the inner plexiform layer (IPL), consistent with an identity as ON BPs (Connaughton

and Nelson, 2000), or in both the inner and outer halves of the IPL, consistent with an identity as Mixed ON/OFF BPs (Connaughton and Nelson, 2000) (Fig. 2.1A,D). The *nyx::mYFP+* and PKCα+ BPs were destroyed by the ouabain lesion, as observed at three days post-injury (3 DPI) in sectioned eyes (Fig. 2.1B,E,F), and by microscopic observation of the YFP reporter in eyes of live, anaesthetized fish (data not shown).

Viability of photoreceptors in lesioned retinas was confirmed for all four morphological subtypes of cones, using a GFP reporter driven by the SWS1 opsin promoter (UV cones) (Takechi et al., 2003) (Fig. 2.1A-C), the antibody ZPR1, which stains cone arrestin 3a (arr3a) in red- and green-sensitive double cones (DCs) (Renninger et al., 2011) (Fig. 2.1A-E), and an mCherry reporter driven by the SWS2 opsin promoter (blue cones) (Takechi et al., 2008) (Fig. 2.1). Cones retained their characteristic morphologies at the 3 DPI sampling time (Fig. 2.1), similar to the findings after selective ablation of xfz43 BPs in larval zebrafish (D'Orazi et al., 2016), but remarkable given the widespread destruction of inner retinal neurons in the present study. The loss of BPs throughout the retina, but the preservation of cones, was consistently observed in lesioned samples sectioned at 3 DPI (Fig. 2.1F) or observed live by fluorescence stereomicroscopy (not shown), confirming 2 µM ouabain as a reliable method to destroy bipolar cells (Fimbel et al., 2007; Nagashima et al., 2013; Sherpa et al., 2014). To analyze the morphologies and connectivities of regenerated BPs, we selected 60 DPI as the time of analysis, because we have previously demonstrated that in addition to histological regeneration, simple, visually-mediated reflexes and behaviors are restored by 60 DPI (Sherpa et al., 2014). Densities of *nyx::mYFP* BPs were evaluated in control retinas, and in regenerated retinas at 60 DPI, and the average number of YFP+ profiles was not significantly different (Fig. 2.1G,H,I; p=0.117; paired, two-sided t-test). Densities of PKCα+ BP neurons were also not significantly reduced following regeneration (Fig. 2.1 p=0.7372; Welch's one-sided t-test).

Although bipolar cells are successfully regenerated following selective lesion, we and others have observed histological abnormalities in regenerated retina, including ectopic cell bodies within plexiform layers [laminar fusions (Hitchcock et al.,

1992; Sherpa et al., 2014)], the production of supernumerary neurons (Sherpa et al., 2011; Sherpa et al., 2014; Powell et al., 2016), and/or neuronal cell types that were not the types injured by the initial damage (Powell et al., 2016). In the present study, IPL layer thickness was significantly reduced at 60 DPI compared to controls (27.7µm ± 2.4 vs. 15.7 µm ± 3.7; p=0.027), and the total length of PKCα+ BPs was also reduced at 60 DPI (60.8 µm ± 4.0 vs. 44.6 µm ± 4.7; p=0.030). Interestingly, there were no differences in the length of the BP neurons when the IPL was subtracted from the measurements (33.12 µm ± 2.0 vs. 28.94 µm ± 3.3; p=0.172, one-sided, two sample t-test), indicating that the primary histological abnormalities may reside within the IPL. Some regenerated PKCα+ BPs showed apparently unusual axon morphologies (Fig. 2.1C). Therefore, we carried out detailed morphometric analyses on a subset of BPs, to test the hypothesis that regenerated BPs restored morphologies and connectivities similar to those of their undamaged counterparts, despite these histological disruptions.
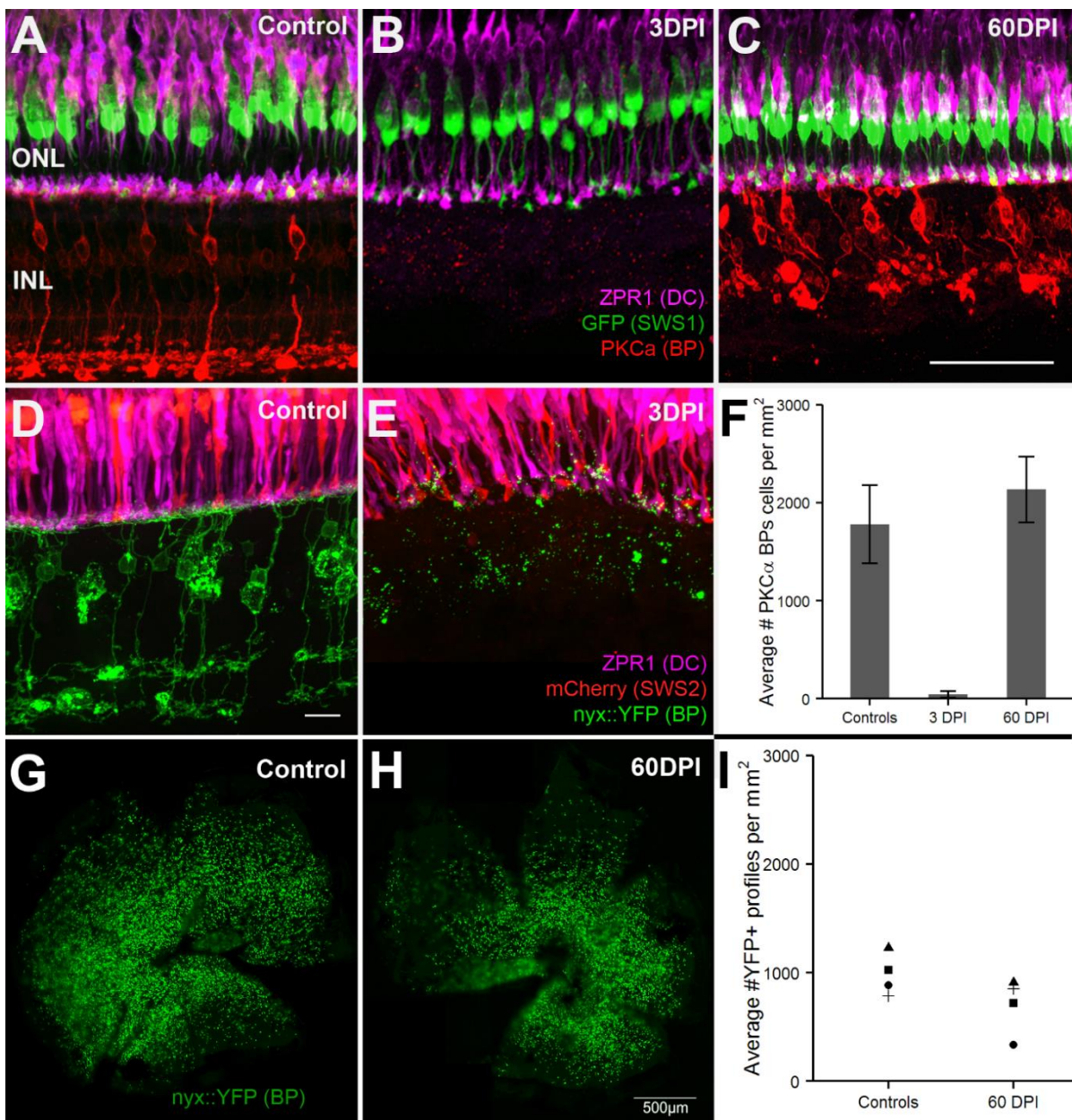
Figure 2.1. Intravitreal 2 µM ouabain destroys retinal bipolar neurons (BPs), spares cone photoreceptors, and permits regeneration of BPs. A. Undamaged retina showing ZPR1+ double cones (DCs), UV (SWS1) cones, and PKCα+ BPs. B. Damaged retina at 3 days post-injury (DPI) showing loss of BPs and persistence of cones. C. Damaged, and then regenerated retina at 60 DPI (days post-injury) showing regenerated BPs; arrow indicates a BP axon lacking the typical, straight trajectory. D. Undamaged retina showing ZPR1+ DCs, blue (SWS2) cones, and *nyx::YFP*+ BPs. E. Damaged retina at 3DPI showing loss of BPs and persistence of cones. F Quantification (mean ± SEM) of PKCα BPs in cryosections; they are destroyed by 3 DPI and normal density is restored by 60 DPI (p=0.7372). G,H. Low magnification images of flat-mounted, *nyx::mYFP* control retina (G) and regenerated retina (H), showing distribution of YFP+ profiles. I. Scatterplots showing quantification of YFP+ profiles in undamaged and 60 DPI regenerated retina of contralateral eye. Each symbol represents a retina from a separate fish (p=0.117). ONL, outer nuclear layer; INL, inner nuclear layer. Scale bar in C (applies to A-E) = 50 µm.

Complexity of dendritic trees of regenerated nyx::mYFP bipolar neurons is restored.

To analyze dendritic tree morphologies of BPs we took advantage of the variegated expression of the mYFP reporter in the adult *nyx::mYFP* transgenic zebrafish (Schroeter et al., 2006; Saade et al., 2013), as this permitted the visualization of individual BPs in retinal whole mounts by confocal microscopy. The dendritic area of traced BPs was measured by drawing a convex polygon around the perimeter of the dendritic tree (Kraft et al., 2006), and separately by fitting an ellipse around the perimeter of the dendritic tree (Li et al., 2012) (Fig. 2.2A,B). These measurements revealed median dendritic spreads of 200-250 µm2 (Fig. 2.2A; polygon), and 350-400 µm2 (Fig. 2.2A; ellipse) for both sample populations. Both measures did not detect a significant difference in dendritic spread of regenerated BPs (n=26) as compared with undamaged control BPs (n=26) ($p=0.25$ for polygon; $p=0.44$ for ellipse; Kruskal-Wallis rank sum test) (Fig. 2.2A). Control and 60 DPI dendritic spreads showed similar Feret's diameters ($p=0.865$; n=25 and 26; Kruskal Wallis) with median diameters of 23.9 µm and 25.0 µm, respectively. Control and 60 DPI dendritic spreads also were similar in roundness ($p=0.441$; n=26; Welch's two sided t-test) with mean values ± SEM of 0.738 ± 0.037 and 0.701 ± 0.0277, respectively.

Sholl analysis (Sholl, 1953) was used as an additional measure of morphology and complexity of dendritic trees of identified *nyx::mYFP* BPs. Sholl analysis measures the number of dendritic branches that intersect a series of concentric circles drawn at increasing distance from a defined centerpoint of the dendritic network (Fig. 2.2C). Outputs of Sholl analysis provide quantitative information regarding the density of branches, distribution of branches, and branching pattern of the dendritic tree of identified neurons. This analysis revealed no differences in the Sholl regression coefficients (Fig. 2.2C; $p=0.1484$) and Y-intercepts (data not shown; $p=0.1621$) using the semi-log method, in regenerated *nyx::mYFP* BPs as compared with control *nyx::mYFP* BPs (Kruskall-Wallis rank sum test; n=21 for controls; n=23 for 60 DPI). In addition, output of Sholl analysis using the linear method also showed no significant differences in regenerated *nyx::mYFP* BP dendritic tree morphologies as compared with controls (Table 2.1; data not shown).
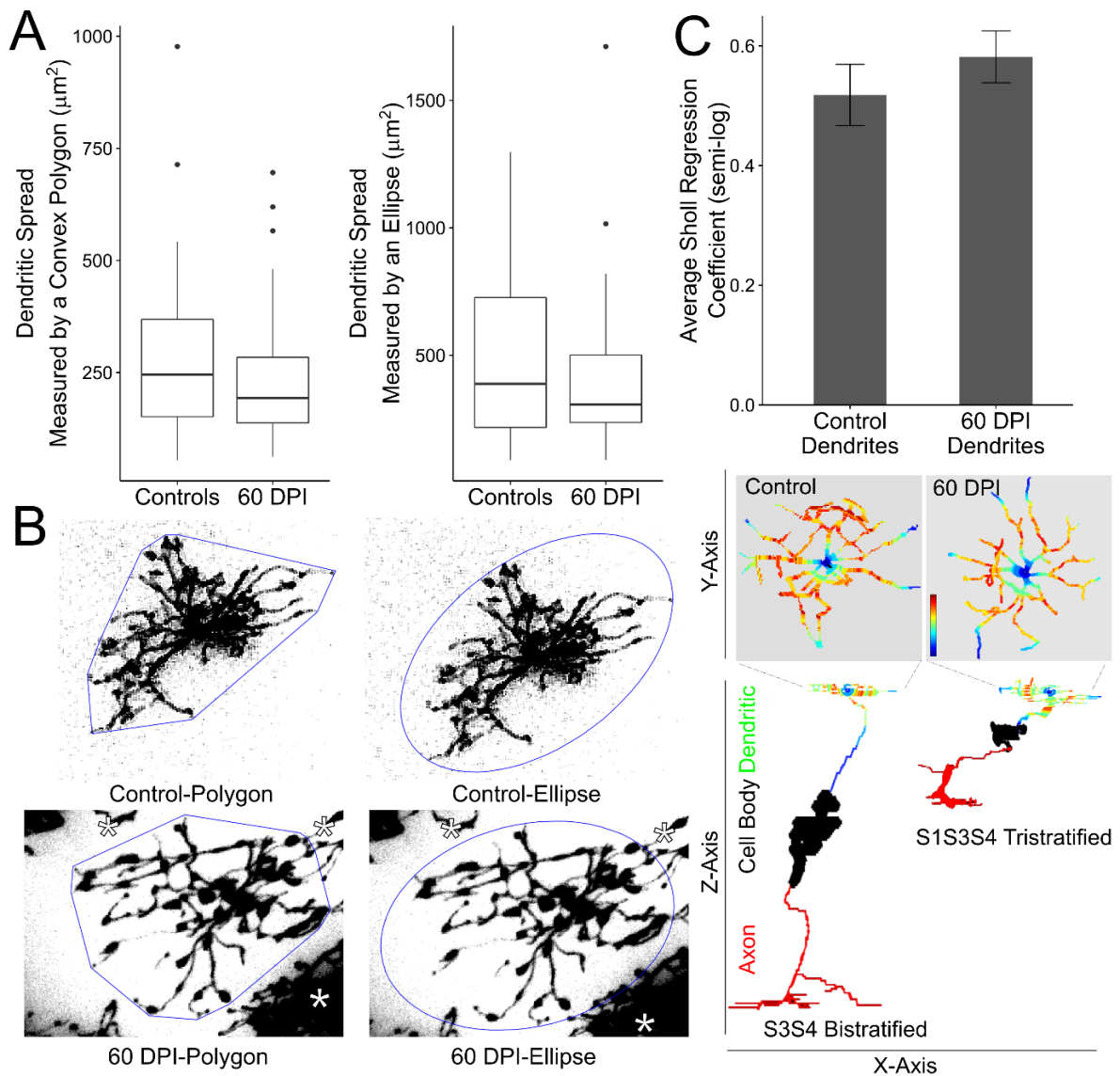
Figure 2.2. Dendritic field sizes and complexities of *nyx::mYFP* bipolar neurons (BPs) are restored in regenerated retina. A. Boxplots showing distribution of dendritic field sizes as measured by convex polygons or by ellipses. In the boxplots, the band inside the box represents the median, the top and bottom of the box represent the 25th and 75th percentiles, the whiskers represent the 1.5 interquartile range, and the filled circles represent outliers. B. Convex polygons and ellipses (blue) drawn around the dendritic fields of examples of control and regenerated BPs. C. Sholl analysis of complexity of dendritic trees of control and regenerated *nyx::mYFP* bipolar neurons (BPs).Top: Mean (± SEM) Sholl (semi-log) regression coefficients for BPs in control and regenerated retinas. Bottom: X-Z views of selected, traced BPs. Top (Y-axis) view of dendritic trees are color-coded by heatmaps to demonstrate relative numbers of dendrite branches that cross circles of increasing distance from the initial branch point. Hotter colors represent more dendrites, while cooler colors represent fewer dendrites. DPI, days post-injury; asterisks (*) indicate dendrites of neighboring *nyx::mYFP* BPs.

Cone connectivity patterns of regenerated nyx::mYFP bipolar neurons are restored.

To determine the cone connectivity patterns of BPs, identified *nyx::mYFP* BPs were visualized in retinal whole mounts together with blue-sensitive cones (SWS2:mCherry) and ZPR1-stained DCs (Fig. 2.3A,B). Several samples permitted further discrimination of the red- vs. green-sensitive (LWS vs. RH2 opsin-expressing) members of each DC pair, because the ZPR1 antibody more strongly labeled the red-sensitive (LWS) member (Fig. 2.3A,B). Furthermore, the organization of the cone mosaic in adult zebrafish retinas permits the assignment of red vs. green in regions where clearly aligned rows of DCs display alternating orientations (Allison et al., 2011; Li et al., 2012). Connectivity assignments were made using image stacks that included traced (Fig. 2.3A-F) and untraced (Fig. 2.3G,H) *nyx::mYFP* BPs, supervised assignment of cone terminal identity (Fig. 2.3E,F), and verification of dendritic tip (endpoint) association with cone terminals (Fig. 2.3G,H). Assignments and assessments of cone-BP synapses were in many cases further verified in X-Z projections (Fig. 2.3A`-H`). Regenerated *nyx::mYFP* BPs made connections to all of the identified cone subtypes, similar to the range of connections made by undamaged control *nyx::mYFP* BPs (Table 2.2).

A — Control

SWS2
traced nyx::mYFP (BP)
ZPR1+ (DC)

A`

B — 60 DPI

r g
g r
b b

B`

Dendrite
Axon
Nuclei
Soma

C

untraced
nyx::mYFP (BP)

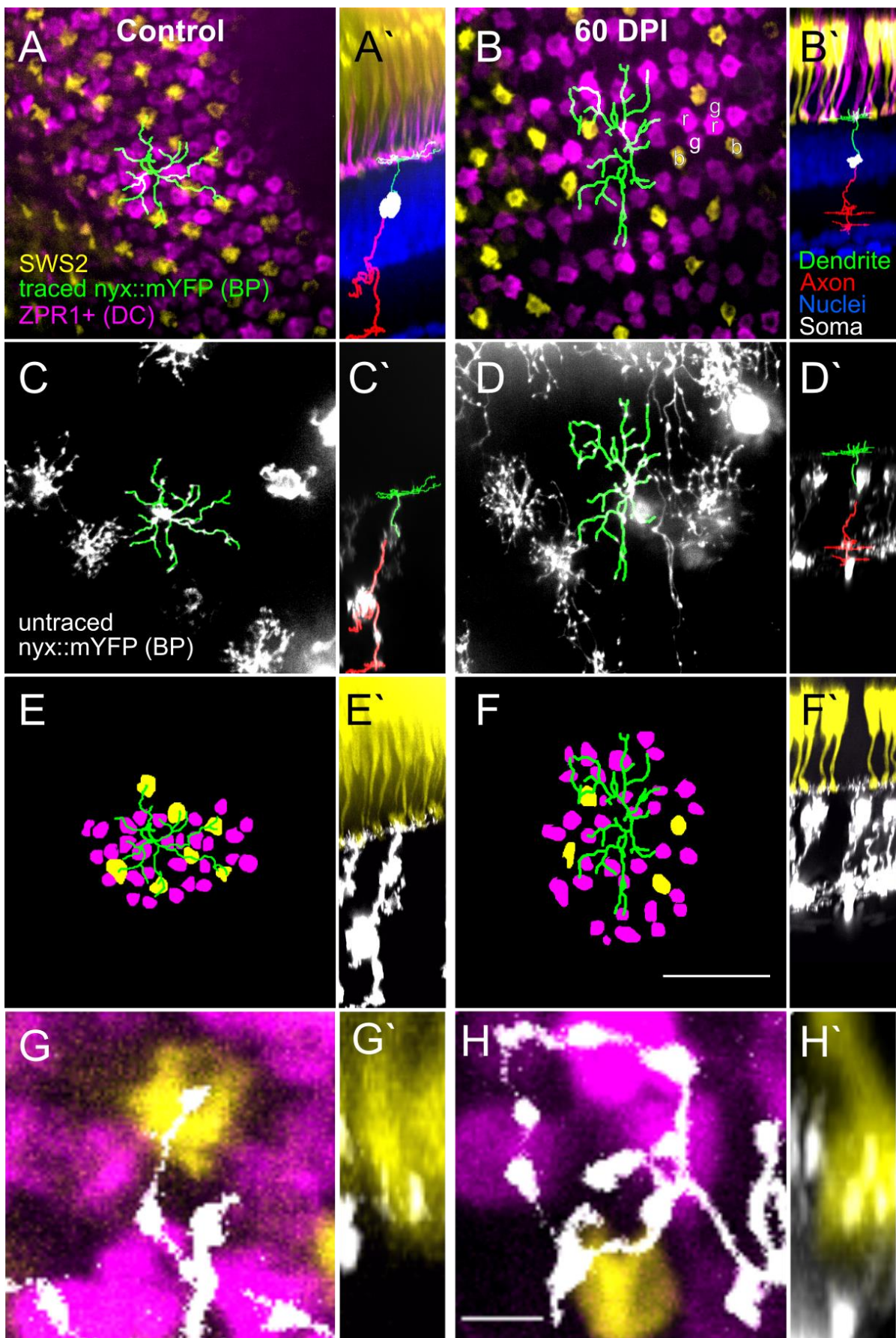C`

D

D`

E

E`

F

F`

G

G`

H

H`

Figure 2.3. Determination of cone connectivity patterns of *nyx::mYFP* bipolar neurons (BPs) in control and regenerated retinas. A,B. Traced individual BP dendritic fields, overlaid with view of synaptic terminals of blue-sensitive (SWS2; b in panel B), and ZPR1+ double cones (DC) in control (A) and regenerated (B) retinas. Position in cone mosaic and more intense labeling of red-sensitive cones (LWS; r in panel B) permits their identification as distinct from the green-sensitive cones (RH2; g in panel B). C,D. Traced individual BP dendritic fields overlaid by the microscopic image showing examples of untraced BPs in control (C) and regenerated (D) retinas. E,F. Traced individual BP dendritic fields overlaid with traced cone terminals in control (E) and regenerated (F) retinas. G,H. Higher magnification Z-projections to show dendritic tips associated with cone terminals. A`-H` depict partial projections from image stacks to show resliced radial view of analyzed BPs. Scale bar in F (applies to A-F) = 20 µm; scale bar in H (applies to G,H) = 2.5 µm.

Parameter	P value (control vs. 60 DPI)	Statistical test
Maximum # of intersections	0.325	Kruskal-Wallis
Sum of intersections	0.685	Kruskal-Wallis
Radius at maximum # of intersections	0.469	Kruskal-Wallis
Critical value	0.780	Welch's 2-sample t-test
Radius of critical value	0.418	Kruskal-Wallis
Enclosing radius	0.158	Welch's 2-sample t-test
Kurtosis of the sampled data	0.799	Kruskal-Wallis
Kurtosis of the fitted data	0.817	Welch's 2-sample t-test
Skewness of the sampled data	0.856	Welch's 2-sample t-test
Skewness of the fitted data	0.872	Welch's 2-sample t-test

Table 2.1. Sholl analysis of dendrite branding patterns of *nyx::mYFP* bipolar neurons in control and regenerated retinas.

Connectivities[1]	Relative numbers of endpoints[2]	Number of neurons	
		Control	60 DPI
BGRX	Low	1	0
	Medium	7	3
	High	2	3
BGX	Low	1	0
	Medium	1	0
BRX	Medium	0	2
GRX	Medium	1	1
	High	0	1
GX	Low	0	1

Table 2.2. Connectivity patterns of *nyx::mYFP* bipolar neurons observed in control and regenerated retinas.
[1] Connections observed to SWS2 (B), RH2 (G), and LWS (R) cones, as well as unassigned (X) connections.
[2] Low, 10 or fewer total endpoints; Medium, 11-20 total endpoints; High, over 20 total endpoints.

The numbers of dendritic tips of each identified *nyx::mYFP* BP neuron were not significantly different in regenerated vs. control retinas (Fig. 2.4A; p=0.6062; Welch's two-sided t-test). The total number of endpoints per neuron ranged from 7 to 30, similar to ranges observed previously (Li et al., 2012).

Cone connectivity patterns were analyzed further to test whether the number of connections regenerated *nyx::mYFP* BPs made to each type of cone were similar or different than those of control *nyx::mYFP* BPs. Unassigned connections were most likely connections to UV cones or rods (Li et al., 2012), but we cannot rule out the possibility of endpoints lacking connections. Figure 2.4 plots the distributions of assigned cone-specific connections, as well as unassigned/presumed UV or rod connections. We used a generalized linear model (GLM) to determine if these connectivity patterns are significantly different between control and 60 DPI retinas, such that the *nyx::mYFP* BPs more or less often connect to blue sensitive cones, green sensitive cones, red sensitive cones, and unassigned in a regenerated retina. The strength of the GLM is that it allows for response variables that are not linear. Here, because our response variable, cone-specific connections, is count data we used the Poisson distribution. The features of these distributions are indeed statistically similar (p = 0.453). Therefore, the regenerated *nyx::mYFP* BPs developed dendritic trees that received input from similar combinations of cones (Table 3) and displayed similar numbers of connections to each cone subtype (Figure 2.4).

Stratification Layers	Predicted Function	Number of Neurons	
		Control	60 DPI
S4S5	ON		3
S5		1	3
S5S6		1	
S6		1	
S1S6	Mixed ON/OFF	1	
S1S3S6		1	2
S2S4			1
S2S5		1	1
S2S6		2	
S3S4		1	
S3S5		1	
S3S6		1	4
S4S5S6			1

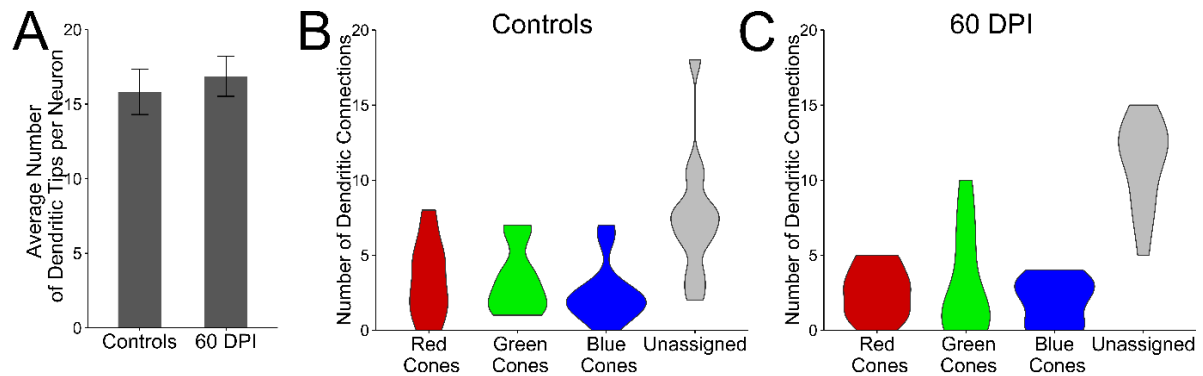Table 2.3. Axon stratification patterns of *nyx::mYFP* bipolar neurons in control and regenerated retinas.

Figure 2.4. Re-establishment of BP dendritic connections with photoreceptors. A. Column graph showing average number of dendritic tips per *nyx::mYFP* BP in control and regenerated retina. B,C. Distributions of dendritic connections to identified and unassigned photoreceptor subtypes for *nyx::mYFP* bipolar neurons in control (B) and regenerated (C) retinas. Shapes of violin plots were obtained by using a kernel density estimator to generate a smoothened histogram, mirrored along the x-axis, and then rotated. The width of each plot is determined by the proportion of bipolar cells making a given number of connections to that photoreceptor subtype at that point.

Synaptic connections to cones are also restored in regenerated PKCα+ bipolar neurons.

To further test for the restoration of cone-BP synapses in retina that regenerated following destruction of inner retinal neurons, we visualized PKCα+ BPs in sectioned retinas. The PKCα+ BP population is too dense to visualize as individual neurons in whole mounts, but offers versatility for multi-color confocal imaging in sectioned retinas together with UV-sensitive (SWS1) cones that are GFP+. We also verified that a synapse-specific marker, SV2 (synaptic vesicle 2) (Yazulla and Studholme, 2001) was present and properly localized in regenerated adult retina. In

undamaged control retinas, SV2 was localized to the OPL and IPL (Fig. 2.5A), and UV-sensitive (SWS1:GFP) cones made apparent synaptic contacts with PKCα+ BPs (Fig. 2.5A,D,G). At 3 DPI, an SV2+ IPL was not detectable, while the OPL was still stained by SV2 (Fig. 2.5B). Interestingly, SV2 staining in the 3 DPI photoreceptor layer was more broadly distributed, and appeared to stain some photoreceptor axons as well as axon terminals (Fig. 2.5B and 2.5B inset). This finding indicates that, despite their apparently normal morphology, zebrafish cone photoreceptors may change at the subcellular level in response to injuries that destroy their synaptic partners. To our knowledge, this is the first reported indication of such a change. However, these cone terminals still displayed synaptic clefts (Fig. 2.5E,H). At 60 DPI, the SV2 staining pattern was largely restored, supporting the hypothesis that the regenerated cone-BP synapses are likely functional, although some gaps in the IPL were present, and occasional labeling of structures beyond the OPL was observed (Fig. 2.5C). At 60 DPI, UV cone contacts with PKCα+ BPs were observed (Fig. 2.5F,I). Cone-BP contacts between ZRP1+ DCs and PKCα BPs were also observed to be present in control retinas, lost at 3 DPI, and then restored at 60 DPI (Fig. 2.5J-L).
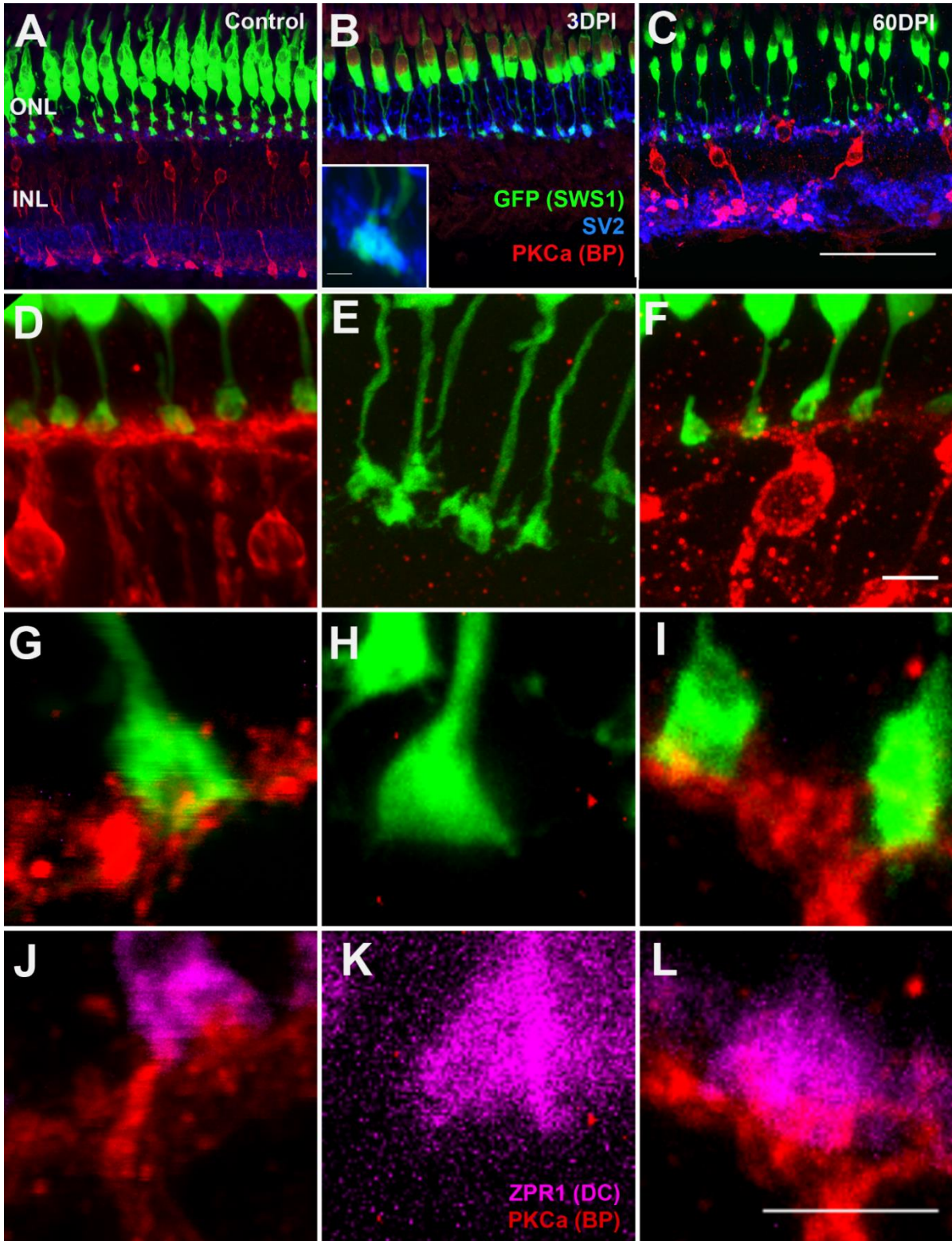
Control — A

ONL

INL

3DPI — B

GFP (SWS1)
SV2
PKCa (BP)

60DPI — C

D   E   F

G   H   I

J   K   L

ZPR1 (DC)
PKCa (BP)

Figure 2.5. Restoration of synapses between cone photoreceptors and PKCα+ bipolar neurons (BPs) in regenerated retina. A-C. Distribution of presynaptic marker SV2 in undamaged retina (A) and in damaged retinas 3 days post-injury (DPI) (B), and 60 DPI (C). Inset in B shows SV2 immunofluorescence associated with a UV-GFP terminal. D-F. PKCα+ BPs are absent at 3 DPI (E) but regenerated with connections to GFP+ UV (SWS1) cones at 60 DPI (F). G-I. Higher magnification views of UV cone synaptic terminals in control (G), 3 DPI (H), and 60 DPI (I) retinas, showing loss and restoration of synapses with PKCα+ BPs. J-L. High magnification views of ZPR1+ double cone (DC) synaptic terminals. ONL, outer nuclear layer; INL, inner nuclear layer. Scale bars in C (applies to A-C), F (applies to D-F), and L (applies to G-L) =5 µm.

Axons of regenerated nyx::mYFP bipolar neurons display a diversity of stratification patterns and complexities.

Using the X-Z projections of identified *nyx::mYFP* BPs in imaged whole mounted retinas (Fig.2. 6A,B), we next tested whether axons of regenerated BPs displayed the same diversity of stratification patterns in the IPL as their undamaged counterparts. BP neurons of the zebrafish can show a variety of stratification patterns, each likely indicative of function as either an ON BP (synapsing in deep layers, S4-S6), an OFF BP (synapsing closer to the INL, S1-S3), or a mixed ON/OFF BP (synapsing in a combination of these layers) (Connaughton and Nelson, 2000; Connaughton et al., 2004). The stratification patterns of *nyx::mYFP* BPs in control retinas revealed some diversity, with individual neurons showing distinct stratification combinations. Analyzed BPs showed mono-, di-, and tri-stratified axon morphologies (Fig. 2.6; Table 2.3). The majority could be tentatively assigned to a function as a mixed ON/OFF BP. Although the IPL of regenerated retinas showed reduced thickness, regenerated *nyx::mYFP* BPs also displayed a diversity of apparent stratification patterns that could tentatively be designated with functional assignments as mixed ON/OFF BPs (Table 3). The regenerated *nyx::mYFP* BPs did include some distinct patterns not seen in the sample set derived from control retinas (Table 3). However, statistical analysis revealed that the number of stratifications of regenerated BPs matched those of control retinas (generalized linear model; p=0.868), and the types of stratifications (ON vs. mixed ON/OFF) were also similar (Fig. 2.6C; p=0.6823; Fisher's exact test). We conclude that more than a single type of stratification pattern were restored in the regenerated *nyx::mYFP* BPs, and that highly abnormal stratification patterns did not emerge.

Sholl analysis (Sholl, 1953), using the log-log method, found no differences in the Sholl regression coefficient of axons from control vs. regenerated *nyx::mYFP* BPS (Fig. 2.6D; p=0.8537; Welch's two-sided t-test). In addition to using the log-log method, axons were also analyzed using the linear method (Ferreira et al., 2014). Of the output metrics measured, only the maximum number of intersections was significantly reduced in regenerated BPs as compared with control BPs (Table 4). Since there was no difference in the total number of intersections, the size of the overall area occupied by the axon, or the distribution of the axon branches, this finding suggests that axon branches of regenerated BPs are more evenly distributed along the length of the axon (its enclosing "Sholl sphere") than those of control retinas.

Parameter	P value (control vs. 60 DPI)	Statistical test
Maximum # of intersections	0.033	Kruskal-Wallis
Sum of intersections	0.433	Kruskal-Wallis
Radius at maximum # of intersections	0.780	Kruskal-Wallis
Critical value	0.473	Welch's 2-sample t-test
Radius of critical value	0.378	Kruskal-Wallis
Enclosing radius	0.894	Welch's 2-sample t-test
Kurtosis of the sampled data	0.889	Kruskal-Wallis
Kurtosis of the fitted data	0.889	Kruskal-Wallis
Skewness of the sampled data	0.679	Welch's 2-sample t-test
Skewness of the fitted data	0.712	Welch's 2-sample t-test

Table 2.4. Sholl analysis (linear) of axons of *nyx::mYFP* bipolar neurons in control and regenerated retinas.
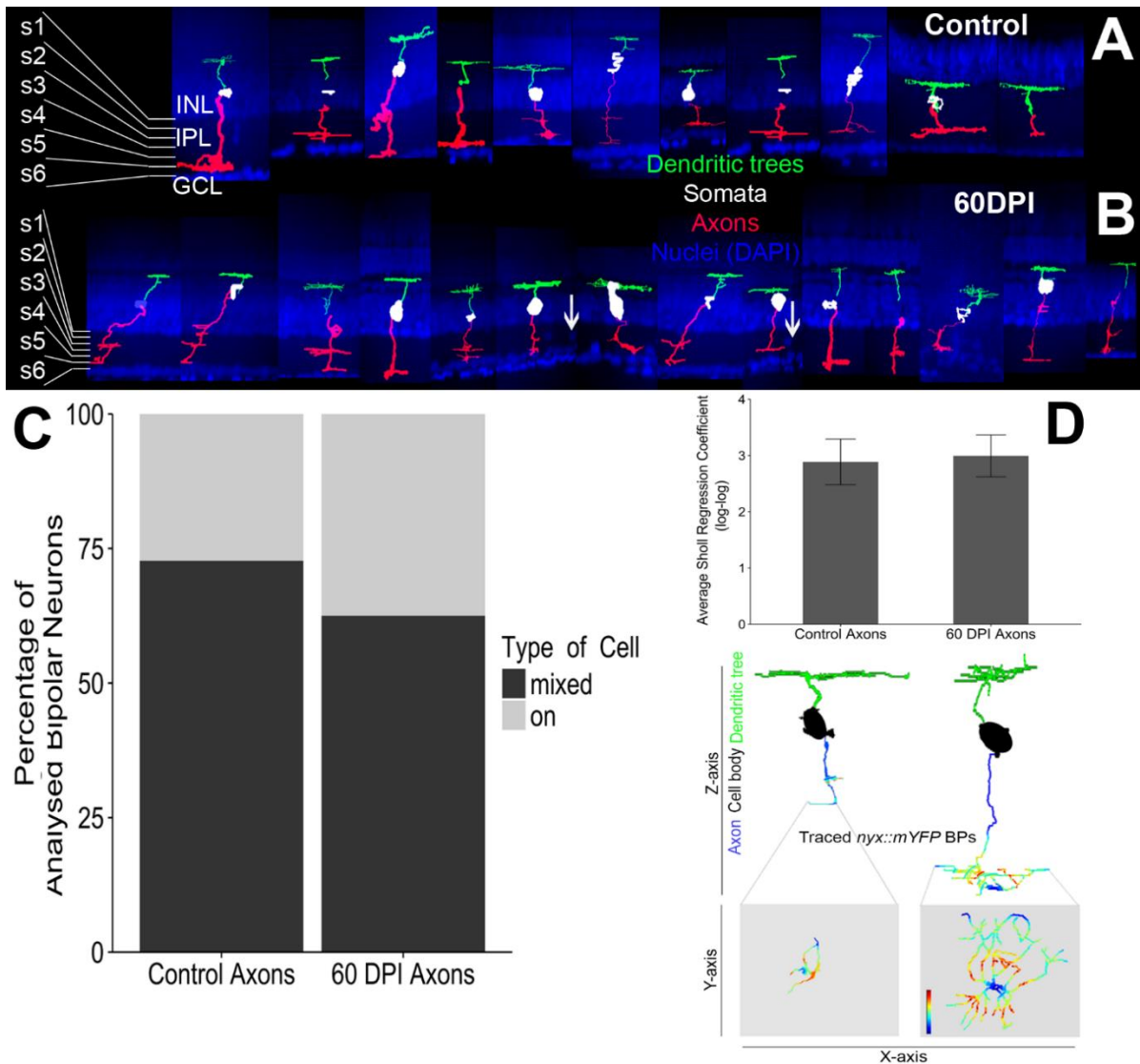
Figure 2.6. Stratification patterns and axon complexities of *nyx::mYFP* bipolar neurons (BPs) are restored in regenerated retina. A,B. X-Z reconstructions of traced *nyx::mYFP* bipolar neurons (BPs). BPs were traced, colorized, and image stacks were resliced with the nuclear marker DAPI to show retinal laminae in control (A) and regenerated (B) retinas. The IPL was divided into 6 equal layers, or strata. INL, inner nuclear layer; IPL, inner plexiform layer; GCL, ganglion cell layer; s1-s6, strata of IPL. Arrows in B show selected examples of "laminar fusions" (nuclei in IPL) regularly seen in regenerated retinas. Sholl analysis of complexity of dendritic trees of control and regenerated *nyx::mYFP* bipolar neurons (BPs). C. Proportions of ON vs. Mixed ON/OFF bipolar neuron (BP) identities assigned based upon axon stratification patterns of *nyx::mYFP* BPs in control and regenerated retinas. D. Top: Mean (± SEM) Sholl (log-log) regression coefficients for BPs in control and regenerated retinas. Bottom: X-Z views of selected, traced BPs. Bottom (Y-axis) views of axon branching patterns are color-coded by heatmaps to demonstrate relative numbers of axonal branches that cross circles of increasing distance from the initial branch point. Hotter colors represent more axons, while cooler colors represent fewer axons.

Combinations of morphologies of nyx::mYFP bipolar neurons are restored.

   We next tested whether combinations of dendritic or axon parameters displayed distinct covariances in regenerated vs. control BP populations, which would suggest differential biases in the production of *nyx::mYFP* BPs with specific functional attributes. We found that dendritic spread was not differentially correlated with dendritic complexity (Sholl regression coefficient), dendritic spread was not differentially correlated with axon complexity, dendritic complexity was not differentially correlated with axon complexity, and the number of dendritic endpoints was not differentially correlated with axon complexity (Table 2.5; Fig. 2.7A-C). Therefore, regenerated BPs showed no biases favoring particular combinations of morphologies, and did not demonstrate a lack of combinations/correlations observed in undamaged BPs. Visualization of three distinct morphological measurements – dendritic spread, total number of endpoints, and the Sholl regression coefficient for axons (log-log) – using 3-D scatterplots, also did not reveal any differential clustering in regenerated vs. control BPs (Fig. 2.7D).

Variable 1	Variable 2	p-value[1]
Dendritic field size (ellipse)	Dendritic complexity (Sholl regression, semi-log)	1.0
Dendritic field size (polygon)	Dendritic complexity (Sholl regression, semi-log)	0.6682
Dendritic field size (ellipse)	Max intersections of dendrites (Sholl linear)	0.8864
Dendritic complexity (Sholl regression, semi-log)	Axon complexity (Sholl regression, log-log)	0.8815
Total dendritic endpoints	Axon complexity (Sholl regression, log-log)	0.8815
Dendritic field size (ellipse)	Axon complexity (Sholl regression, log-log)	0.1797

Table 2.5. Pairwise analysis of continuous variables representing dendrite and axon morphologies of *nyx::mYFP* bipolar neurons in control and regenerated retinas. [1]Kruskal-Wallis rank sum test of regression coefficients.
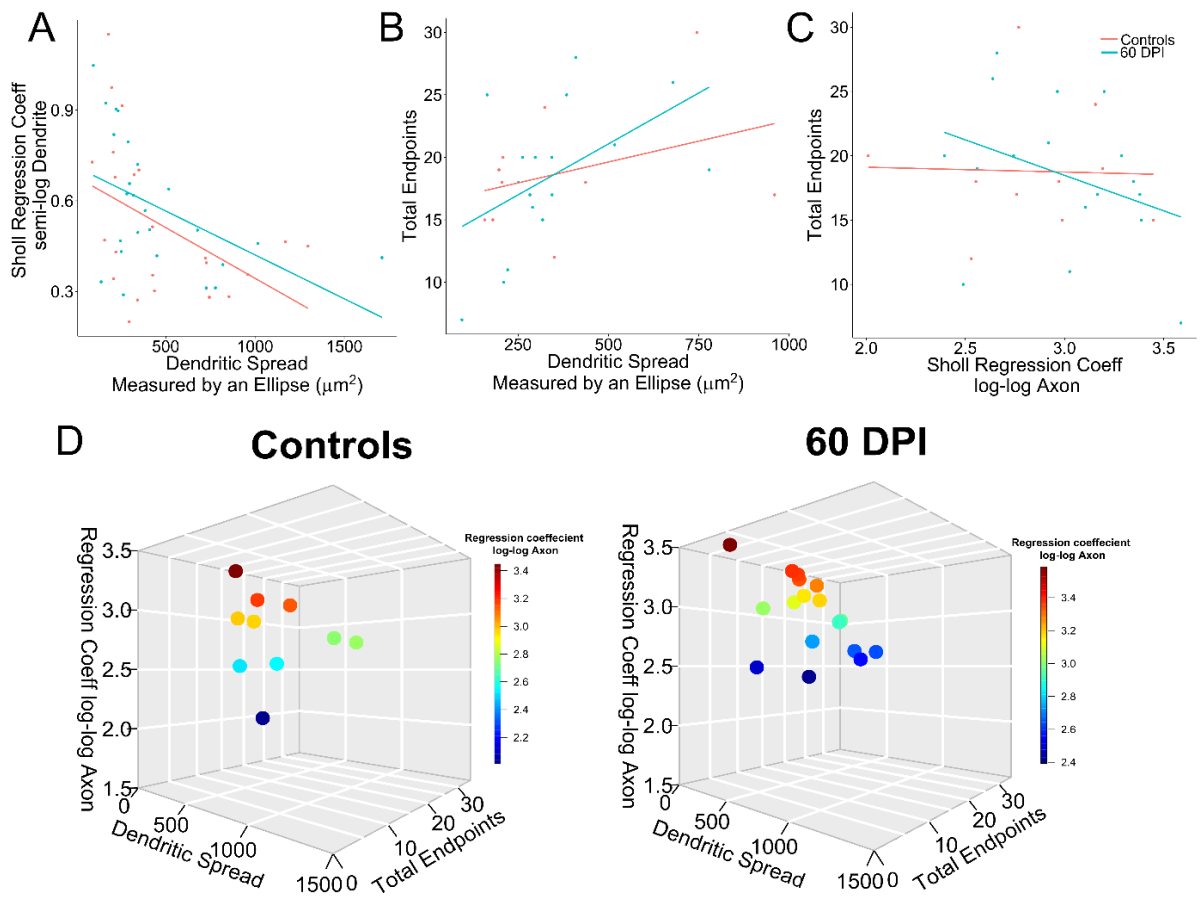
Figure 2.7. Correlations of morphometric parameters of control and regenerated *nyx::mYFP* BPs. A. Dendritic complexity (Sholl regression coefficient, semi-log) is not differentially correlated with dendritic spread (ellipse method) in control vs. regenerated BPs. Controls, R2=0.157; 60 DPI, R2=0.223 (R2 values for these graphs calculated by simple linear regression that does not account for individual fish). B. Number of dendritic endpoints is not differentially correlated with dendritic spread in control vs. regenerated BPs. Controls, R2=0.058; 60 DPI, R2=0.230. C. Number of dendritic endpoints is not differentially correlated with axon complexity (Sholl regression coefficient, log-log) in control vs. regenerated BPs. Controls, R2=0.000; 60 DPI, R2=0.119. D. Visualization of three morphological parameters of BPs in control retinas and in regenerated retinas at 60 DPI shows that the two BP populations occupy similar regions of the 3-D space. DPI, days post-injury.

Because our morphometric analyses did not reveal substantial, statistically significant differences in sizes or complexities of dendritic trees or axons, or in connectivities of BPs in the two experimental conditions, we also assessed BP morphologies qualitatively. Projected surface renderings are shown in Fig. 2.8, from several different viewpoints. Our conclusion from qualitative inspection of these projections, is that the regenerated BPs show a range of morphologies that are largely similar to the range of morphologies of control BPs, suggesting a lack of bias in the production of any one morphology during retinal regeneration.
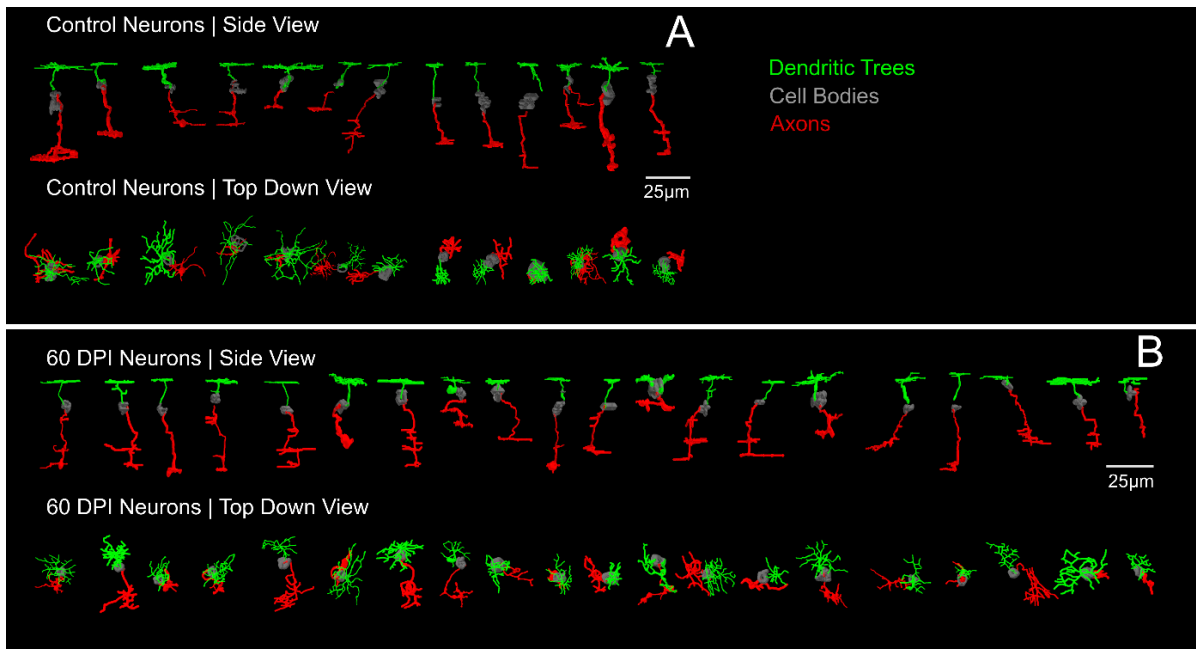
Figure 2.8. Surface renderings of control (A) and regenerated (B) *nyx::mYFP* bipolar neurons.

Discussion

We provide the first detailed quantitative and qualitative report of bipolar neuronal morphologies and predicted circuitry in regenerated adult zebrafish retina following destruction of multiple neuronal types. The major conclusions are: 1) morphologies and complexities of dendritic trees of regenerated *nyx::mYFP* BP neurons are similar to those within undamaged retina; 2) cone connectomes of regenerated BP neurons are restored; 3) axon terminal stratification and branching patterns of regenerated *nyx::mYFP* BPs show only minor differences as compared to those within undamaged retina; and 4) *nyx::mYFP* BPs in regenerated retina show morphological diversity, suggesting a lack of bias during regeneration to favor any one BP morphology. These findings suggest that the regenerated retina of adult zebrafish has the underlying anatomical capacity to support complex retinal functions similar to those in undamaged retinas.

Morphologies and complexities of dendritic trees of regenerated BPs are restored.

The lesion used here destroyed inner retinal neurons while sparing photoreceptors and glia (Fimbel et al., 2007; Nagashima et al., 2013; Sherpa et al., 2014) (Fig. 2.1), creating a disrupted retinal environment that could be considered challenging for the growth and elaboration of dendritic processes of regenerating BPs. However, when sampled at a time corresponding to restoration of function (60 DPI) (Sherpa et al., 2014), these neurons displayed dendritic field characteristics that were statistically undistinguishable from their undamaged counterparts. Similarly, dendritic territories of regenerated xfz43 BPs were also restored after cell-selective ablation of this BP subpopulation in larval zebrafish retina, with the exception of regenerated ON T1 xfz43 BPs, which had much larger dendritic trees (D'Orazi et al., 2016). The present study demonstrates that both dendritic field sizes and complexities are restored by adult regenerated *nyx::mYFP* BPs, and that this restoration can take place in a disturbed retinal environment. In adult goldfish subjected to a surgical retinal lesion, dendritic trees of regenerated RGCs were also observed to attain normal structural attributes and modeled electrotonic properties (Cameron et al., 1999). Together with the present study these results support the hypothesis that even within the disrupted environment of damaged retina, new neurons elaborate dendrites that are capable of adequately sampling the visual field and supporting normal retinal processing.

Cone connectomes of regenerated BPs are restored.

The present study shows that dendrites of regenerated *nyx::mYFP* BPs collect synaptic input from multiple cone photoreceptor types, with distributions of connectivities similar to those of *nyx::mYFP* BPs in undamaged retinas. These include connections to SWS2 ("blue"), RH2 ("green"), and LWS ("red") cones. In addition, PKCα+ BPs restored connections to SWS1 (UV) cones and double cones. Similarly, the ultrastructure of regenerated goldfish photoreceptor-bipolar neuron synapses was verified as normal, with presynaptic ribbons and postsynaptic processes restored (Hitchcock and Cirenza, 1994), and amacrine cells within a regenerated region of goldfish retina could functionally integrate with the surrounding

undamaged retina (Hitchcock, 1997). In the current study, retinal BPs were challenged to integrate accurately with undamaged photoreceptors, and all measures of this integration indicate that the regenerated cone-bipolar circuitry could also support normal retinal function.

Following a cell-selective cone lesioning approach in larval zebrafish retina, undamaged H3-type horizontal cells successfully reconnected to regenerated UV cones, except in circumstances when the regeneration of UV cones was delayed or prevented (Yoshimatsu et al., 2016). In the current study, regeneration of inner retinal neurons was allowed to follow a normal time-course, and regenerated BPs appeared to accurately re-wire with cones. It will be important to determine whether delay of BP regeneration also results in faulty re-wiring in adult retinas, and also whether re-wiring is accurate in the more highly disrupted environment of retina following a lesion that destroys all neurons and spares Müller glia (Sherpa et al., 2008). In these regenerated retinas following this more extensive damage, the cone mosaic is extremely disorganized (Stenkamp et al., 2001; Sherpa et al., 2008), and may represent an obstacle for the restoration of cone-BP circuitry.

Also in larval zebrafish retina, regenerated xfz43 BPs were challenged to form circuits with undamaged photoreceptors following cell-selective destruction of only this BP population (D'Orazi et al., 2016). A subset of these BPs, the ON T2 type and the OFF type, showed a slightly reduced bias toward synapsing with LWS cones after regeneration, instead favoring RH2 cones or other photoreceptor types (D'Orazi et al., 2016). Our findings of no differential biases in connectivity of regenerated *nyx::mYFP* BPs suggest that restoration of accurate connectivity patterns may be facilitated by a more robust regeneration process. It is also possible that the photoreceptors of mature zebrafish retina are less plastic and less likely to make connectivity errors than those of growing larval retina. Alternatively, the differential bias observed by D'Orazi et al. (D'Orazi et al., 2016) may be specific for regeneration of the ON T2 and OFF type BP subpopulations.

Axon terminal stratification and branching patterns of regenerated BPs are largely restored.

The damage mode used in the present study provided regenerating BPs with undamaged upstream synaptic partners (photoreceptors), but also with newly regenerated downstream synaptic partners (amacrine cells and RGCs). Furthermore, prior studies of regenerated teleost fish retinas have documented the presence of histological abnormalities in the IPL of regenerated retina, in particular "laminar fusions" – misplaced cell bodies that bridge the INL with the GCL (Hitchcock et al., 1992; Sherpa et al., 2008; Sherpa et al., 2014) (examples in Fig. 2.6B). In the present study we also observed reduced thickness of the IPL. Given these histological disruptions, it was somewhat surprising that the stratification patterns and Sholl regression coefficients of axons of regenerated *nyx::mYFP* BPs were similar to those in undamaged retinas.

The population of BPs most deeply sampled in this study, *nyx::mYFP*, was previously characterized as ON bipolar cells, based upon their axon terminal stratifications in the deep layers of the IPL in larval zebrafish (Bahadori et al., 2006; Schroeter et al., 2006). However, we observed that in adult zebrafish this population is more heterogeneous, such that some *nyx::mYFP* BP axons showed a mixed ON/OFF stratification pattern, with axon terminals in both OFF and ON layers. Furthermore, the *nyx::mYFP* BPs could be mono-, bi-, or tri-stratified. These patterns were reconstituted in retinas that regenerated after lesioning of inner retinal neurons. No regenerated *nyx::mYFP* BPs were found to stratify exclusively in OFF layers, and there were no statistically significant biases in any stratification pattern. These findings suggest that regenerating BPs deployed stratification programs which resulted in the adult patterns rather than recapitulation of the larval patterns. These findings may appear in contrast to those of (Hitchcock and Cirenza, 1994), in which the distribution of synapses within the depth of the IPL were found to be distinct in regenerated goldfish retina (following a surgical lesion), as compared with controls. It is possible that these differences were related to a BP subpopulation that was not sampled in the current study. Alternatively, regeneration following a surgical lesion may result in more errors in finding synaptic partners, than regeneration following

damage of only inner retinal neurons. Further research will be needed to identify the postsynaptic partners of regenerated BPs to determine the accuracy of re-wiring within the IPL.

The axon branching patterns of *nyx::mYFP* BPs in adult zebrafish appeared complex in comparison with the more simple terminals documented in larval zebrafish (Schroeter et al., 2006; D'Orazi et al., 2016). In addition, Sholl analysis indicated that regenerated *nyx::mYFP* BP neurons attained nearly the same complexity as those from undamaged retinas. These findings provide further support that regeneration restores the adult pattern of wiring rather than the larval pattern. Together with the stratification data, these results also indicate the potential for regenerated BP neurons to navigate the disrupted environment to reform native circuitry with amacrine and ganglion cells.

Morphological diversity of regenerated nyx::mYFP BPs is restored.

The complex visual processing functions of the retina require the activities of a diverse array of cellular components, and retinal BP neurons are excellent examples of a structurally and functionally diverse retinal cell population (Connaughton et al., 2004; Li et al., 2012). The *nyx::mYFP* BPs represent this diversity well, with a variety of dendritic morphologies and axon stratification patterns. Remarkably, this range of morphologies, and combinations of morphologies, were restored in regenerated retina. The retinal regeneration process in the adult zebrafish therefore not only restores visually-mediated reflexes and simple behaviors (Sherpa et al., 2008; Sherpa et al., 2014), but also likely regains the underlying circuitry to support complex visual functions. This circuitry is restored despite the disrupted histology of the damaged retina (Hitchcock et al., 1992; Stenkamp et al., 2001; Sherpa et al., 2014; Powell et al., 2016). By comparison with the recent results in larval retina, in which minor connectivity errors were observed for regenerated xfz43 BPs after a cell-specific lesion of these neurons only (D'Orazi et al., 2016), we speculate that some amount of disturbance in the environment of regenerating neurons may perhaps be beneficial, possibly activating mechanisms that facilitate accurate re-wiring. In order to apply these remarkable regenerative capacities to the treatment of human retinal disorders, we must next understand the mechanisms through which regenerating neurons establish accurate synaptic connections.

References

Ahmad I, Del Debbio CB, Das AV, Parameswaran S (2011) *Muller glia: a promising target for therapeutic regeneration.* Investigative ophthalmology & visual science 52:5758-5764.

Allison WT, Barthel LK, Skebo KM, Takechi M, Kawamura S, Raymond PA (2011) *Ontogeny of cone photoreceptor mosaics in zebrafish.* The Journal of comparative neurology 518:4182-4195.

Bahadori R, Biehlmaier O, Zeitz C, Labhart T, Makhankov YV, Forster U, Gesemann M, Berger W, Neuhauss SC (2006) *Nyctalopin is essential for synaptic transmission in the cone dominated zebrafish retina.* The European journal of neuroscience 24:1664-1674.

Bernardos RL, Barthel LK, Meyers JR, Raymond PA (2007) *Late-stage neuronal progenitors in the retina are radial Muller glia that function as retinal stem cells.* J Neurosci 27:7028-7040.

Cameron DA, Vafai H, White JA (1999) *Analysis of dendritic arbors of native and regenerated ganglion cells in the goldfish retina.* Visual neuroscience 16:253-261.

Connaughton VP, Nelson R (2000) *Axonal Stratification Patterns and Glutamate-Gated Conductance Mechanisms in Zebrafish Retinal Bipolar Cells.* Journal of Physiology 524:135-146.

Connaughton VP, Graham D, Nelson R (2004) *Identification and morphological classification of horizontal, bipolar, and amacrine cells within the zebrafish retina.* The Journal of comparative neurology 477:371-385.

D'Orazi FD, Zhao XF, Wong RO, Yoshimatsu T (2016) *Mismatch of Synaptic Patterns between Neurons Produced in Regeneration and during Development of the Vertebrate Retina.* Current biology: CB 26:2268-2279.

Fausett BV, Goldman D (2006) *A role for alpha1 tubulin-expressing Muller glia in regeneration of the injured zebrafish retina.* J Neurosci 26:6303-6313.

Ferreira TA, Blackman AV, Oyrer J, Jayabal S, Chung AJ, Watt AJ, Sjöström PJ, van Meyel DJ (2014) *Neuronal Morphometry Directly from Bitmap Images.* Nature Methods 11:982-984.

Fimbel SM, Montgomery JE, Burket CT, Hyde DR (2007) *Regeneration of inner retinal neurons after intravitreal injection of ouabain in zebrafish.* J Neurosci 27:1712-1724.

Hitchcock PF (1997) *Tracer coupling among regenerated amacrine cells in the retina of the goldfish.* Visual neuroscience 14:463-472.

Hitchcock PF, Cirenza P (1994) *Synaptic organization of regenerated retina in the goldfish.* The Journal of comparative neurology 343:609-616.

Hitchcock PF, Lindsey Myhr KJ, Easter SS, Jr., Mangione-Smith R, Jones DD (1992) *Local regeneration in the retina of the goldfish.* Journal of neurobiology 23:187-203.

Karl MO, Hayes S, Nelson BR, Tan K, Buckingham B, Reh TA (2008) *Stimulation of neural regeneration in the mouse retina.* Proceedings of the National Academy of Sciences of the United States of America 105:19508-19513.

Kraft R, Escobar MM, Narro ML, Kurtis JL, Efrat A, Barnard K, Restifo LL (2006) *Phenotypes of Drosophila Brain Neurons in Primary Culture Reveal a Role for Fascin in Neurite Shape and Trajectory.* The Journal of Neuroscience 26:8734-8747.

Li YN, Tsujimura T, Kawamura S, Dowling JE (2012) *Bipolar cell-photoreceptor connectivity in the zebrafish (Danio rerio) retina.* The Journal of comparative neurology 520:3786-3802.

Longair MH, Baker DA, Armstrong JD (2011) *Simple Neurite Tracer: open source software for reconstruction, visualization and analysis of neuronal processes.* Bioinformatics 27:2453-2454.

Nagashima M, Barthel LK, Raymond PA (2013) *A self-renewing division of zebrafish Muller glial cells generates neuronal progenitors that require N-cadherin to regenerate retinal neurons.* Development (Cambridge, England) 140:4510-4521.

Powell C, Cornblath E, Elsaeidi F, Wan J, Goldman D (2016) *Zebrafish Muller glia-derived progenitors are multipotent, exhibit proliferative biases and regenerate excess neurons.* Scientific reports 6:24851.

Renninger SL, Gesemann M, Neuhauss SC (2011) *Cone arrestin confers cone vision of high temporal resolution in zebrafish larvae.* The European journal of neuroscience 33:658-667.

Saade CJ, Alvarez-Delfin K, Fadool JM (2013) *Rod photoreceptors protect from cone degeneration-induced retinal remodeling and restore visual responses in zebrafish.* J Neurosci 33:1804-1814.

Schindelin J, Arganda-Carreras I, Frise E, Kaynig V, Longair M, Pietzsch T, Preibisch S, Rueden C, Saalfeld S, Schmid B, Tinevez J-Y, White DJ, Hartenstein V, Eliceiri K, Tomancak P, Cardona A (2012) *Fiji: an open-source platform for biological-image analysis.* Nat Meth 9:676-682.

Schroeter EH, Wong RO, Gregg RG (2006) *In vivo development of retinal ON-bipolar cell axonal terminals visualized in nyx::mYFP transgenic zebrafish.* Visual neuroscience 23:833-843.

Sherpa T, Hunter SS, Frey RA, Robison BD, Stenkamp DL (2011) *Retinal proliferation response in the buphthalmic zebrafish, bugeye.* Experimental eye research In press.

Sherpa T, Fimbel SM, Mallory DE, Maaswinkel H, Spritzer SD, Sand JA, Li L, Hyde DR, Stenkamp DL (2008) *Ganglion cell regeneration following whole-retina destruction in zebrafish.* Developmental neurobiology 68:166-181.

Sherpa T, Lankford T, McGinn TE, Hunter SS, Frey RA, Sun C, Ryan M, Robison BD, Stenkamp DL (2014) *Retinal regeneration is facilitated by the presence of surviving neurons.* Developmental neurobiology.

Sholl DA (1953) *Dendritic Organization in the Neurons of the Visual and Motor Cortices of the Cat.* Journal of Anatomy 87:387-406.

Stenkamp DL (2007) *Neurogenesis in the fish retina.* International review of cytology 259:173-224.

Stenkamp DL, Powers MK, Carney LH, Cameron DA (2001) *Evidence for two distinct mechanisms of neurogenesis and cellular pattern formation in regenerated goldfish retinas.* The Journal of comparative neurology 431:363-381.

Suzuki S, Kaneko A (1990) *Identification of bipolar cell subtypes by protein kinase C-like immunoreactivity in the goldfish retina.* Visual Neuroscience 5:223-230.

Takechi M, Hamaoka T, Kawamura S (2003) *Fluorescence visualization of ultraviolet-sensitive cone photoreceptor development in living zebrafish.* FEBS letters 553:90-94.

Takechi M, Seno S, Kawamura S (2008) *Identification of cis-acting elements repressing blue opsin expression in zebrafish UV cones and pineal cells.* The Journal of biological chemistry 283:31625-31632.

Westerfield M (2007) The Zebrafish Book; A guide for the laboratory use of zebrafish (Danio rerio). Eugene, OR: University of Oregon Press.

Wolburg H, Maier W (1979) *Regeneration of the goldfish retina after exposure to different doses of ouabain.* Cell and Tissue Research 202:99-118.

Yazulla S, Studholme KM (2001) *Neurochemical anatomy of the zebrafish retina as determined by immunocytochemistry.* Journal of Neurocytology 30:551-592.

Yoshimatsu T, D'Orazi FD, Gamlin CR, Suzuki SC, Suli A, Kimelman D, Raible DW, Wong RO (2016*) Presynaptic partner selection during retinal circuit reassembly varies with timing of neuronal regeneration in vivo.* Nature communications 7:10590.

CHAPTER 3: Morphological Changes of Bipolar Cells Throughout Key
Time Points of Retinal Regeneration in Zebrafish

Introduction

2µM intravitreal injection of ouabain kills neurons of the inner retina, while
sparing Müller glia, and other unidentified non-neuronal cell types (Raymond, Reifler,
& Rivlin, 1988) (Sherpa, et al., 2014). Fimbel, Montgomery, Burket, & Hyde (2007)
found that most HuC/D+ amacrine and ganglion cell neurons were generated
between 7 and 14 DPI; however, the retina continued to generate HuC/D cells until
60 DPI. This study also utilized selective ablation caused by 2µM ouabain and we
confirmed that both *nyx::mYFP* and PKCα+ bipolar cells were gone by 3 DPI, while
the photoreceptors appeared to remain intact (Figure 2.1). Results from the previous
chapter found that *nyx::mYFP* and PKCα+ bipolar cells in a fully regenerated retina
have similar morphologies to those in an undamaged retina. Results from that
chapter also found that these newly formed bipolar cells reconnect to existing
photoreceptors to reform similar connectivity patterns as the undamaged, control
retinas. However little is known about the morphology of retinal bipolar cells during
the course of regeneration. This study visualized bipolar cells at 13 days post
injection (DPI), 17 DPI, and 21 DPI, measured their morphology, and pattern of
connectivity to existing photoreceptors.

We hypothesize that regenerating bipolar cells of a retina selectively lesioned
by ouabain, partially reform dendrites and axons by 13 DPI. These dendrites and
axons undergo morphological changes throughout regeneration, but overall, have the
same Sholl regression coefficients as the controls, during the 13 to 21 DPI time
points used in this study.

Methods

All methods are identical to those used in Chapter 2 with the exception of what
is specifically stated in this chapter.

All retinas and neurons were also used uninjected controls in Chapter 2.

Animals and retinal lesioning.

Zebrafish used in this study were doubly-transgenic for *nyx::mYFP* and SWS2:mCherry. The *nyx::mYFP* consists of the nyctalopin (nyx) promoter driving gal4, and the UAS enhancer driving expression of yellow fluorescence protein (mYFP) resulting in expression of mYFP in a subpopulation of retinal bipolar neurons (BPs) (Schroeter, Wong, & Gregg, 2006). The SWS2:mCherry transgene results in mCherry expression in blue-sensitive cone photoreceptors (Takechi, Seno, & Kawamura, 2008). In addition, some experiments were carried out on SWS1:eGFP transgenic zebrafish, in which eGFP is expressed in UV-sensitive cones (Takechi, Hamaoka, & Shoji, 2003). Zebrafish were maintained according to Westerfield (2007) in monitored, recirculating system water, on a 14:10 hour light:dark cycle. All procedures using animals were approved by the University of Idaho Institutional Animal Care and Use Committee.

Intraocular injection of ouabain.

Retinas of adult fish were chemically lesioned as previously described (Raymond, Reifler, & Rivlin, 1988) (Sherpa, et al., 2014). Briefly, corneas of anaesthetized fish were perforated to introduce a Hamilton syringe containing 70 µM ouabain in sterile saline; the injected volume (~0.5 µL) resulted in an estimated intraocular concentration of 2 µM. Uninjected contralateral eyes were used as controls. The timing of ablation of BPs, survival of cones, and regeneration of BPs was monitored by observation on some live, anaesthetized fish, at 3-5 DPI using a Nikon SMZ 1500 epifluorescence stereomicroscope.

Imaging and analysis.

Neurons were traced in Fiji using Simple Neurite Tracer (Chapter 2 Methods). These traced neurons were filled using the fill option in SNT, the axon, soma, and dendrite were each converted in an image stack and imported into ImageJ's 3D viewer as surfaces. Each neuron was saved as a separate file in the OBJ format. For Figure 3.3 these OBJ files were imported into 3ds Max 2016, placed together by

their respective time point and then rendered. All text in this figure was generated in Inkscape (ver 0.91). Figure 3.10 was generated using ImageJ's 3D plugin and snapshots were taken of multiple views of these surface rendered neurons. These multiple views were combined in Inkscape to make the final figure.

Sholl analysis was performed on traced BPs to determine the characteristics of individual dendritic trees and axonal branching patterns. This plugin utilized several different variants of the original Sholl Analysis (Sholl, 1953) in order to test for differences in neurons as the retina regenerates. A series of concentric shells (or spheres in this case) are created around a centerpoint. For dendrites used in this study the point at which the primary dendrite branches was considered the center. For axons the point where the primary axon has the largest number of branches was considered the centerpoint. The software counts how many branches cross or intersect at each particular enclosing shell. From those measurements several different regression and mathematical models were generated. The first method is named the linear method and uses a polynomial to best fit the data (Ristanovic, Milosevic, & Stulic, 2006). This calculates the mean number of intersections, sum of intersections, max number of intersections, critical radius and critical value. The polynomial, $N = a + br + cr^2 + dr^3 + er^4 + fr^5 + \cdots + xr^n$ where N is number of intersections, r is the radius, and n is the degree of the polynomial, was used to find the critical value and critical radius. The point where this polynomial function reaches its maximum y-value is known as the critical value and the radius at which the critical value occurs is named the critical radius. The second method is known as the semi-log method, is a type of linear regression analysis. This is done by using the equation $\log\left(\frac{N}{S}\right) = -kr + m$, where N is the number of intersections, S is the shell per volume, r is the radius from the center, k is slope and m is the y-intercept. Since N, S, and r, are known, the slope and y-intercept (m) could be calculated. For this type of analysis, -k is named the Sholl Coefficient. This method was used to compare differences in the dendrites. The third method is known as the log-log method and is also a type of linear regression analysis. This equation uses the function $\log\left(\frac{N}{S}\right) = -k * \log(r) + m$, where N is the number of intersections, S

is the shell per volume, r is the radius from the center, k is slope and m is the y-intercept. As with the second method, N, S, and r, are known, so slope and y-intercept could be calculated. This method was used to compare differences of the axons.

Figures 3.11, 3.12. 3.13, and 3.14 were generated in Imaris version 8.2.0 (Bitplane). Selected neurons were traced using filament tracer. Multiple views were taken in 3D View in order to demonstrate how the neurons are situated within the confocal stack. Pictures showing the top and side views were taken in the Slice View in order to show partially projected top down and side views. In order to see the traced neurons in this module, a new color channel was created by selecting the "create channel from filament" option from the traced axon, and colored red. Another color channel was created for the traced dendrite and colored green.

Statistics.

Data were imported into R Studio (ver 0.99.903) (R Project for Statistical Computing) using R (ver 3.3.1) for statistical analysis.

ANOVAs and Kruskal-Wallis tests were used for parametric and most non-parametric data, respectively. Since none of the parametric data had statistical significance ($p < 0.05$) as measured by a one-way ANOVA, no post hoc-tests were conducted. For any Kruskal-Wallis test that had a p-value of less than 0.05, a post-hoc test was done using a Wilcoxon–Mann–Whitney test with a false discovery rate p-value adjustment. A generalized linear model with a Poisson distribution was applied for analysis of connectivity patterns and anything p values less than $p = 0.05$ waswere considered significant.

Results

Emergence of regenerated BPs following a ouabain lesion.

We previously documented strikingly normal morphologies of regenerated BPs in retinas sampled at 60 days after a ouabain-mediated lesion of inner retinal neurons (Chapter 2). This lesioning strategy has been verified as destroying neurons

of the inner retina by 3 days post-injury (DPI), sparing Müller glia, photoreceptors, and very few horizontal cells (Fimbel, Montgomery, Burket, & Hyde, 2007). At 60 DPI after this lesion, functional recovery of vision is evident (Sherpa, et al., 2014). To gain insights into the process of BP regeneration and the formation of normal BP morphologies, zebrafish subjected to the same type of lesion were sampled at 13, 17, and 21 DPI. This time frame was selected, in part because neurons of all three layers have been generated at this time (Fimbel, Montgomery, Burket, & Hyde, 2007). The loss of BPs and their regeneration was confirmed in lesioned, *nyx::mYFP*; SWS2:mCherry transgenic zebrafish by observation of eyes of live, anaesthetized fish at 3-5 DPI, to check for the initial lesion, then at 10 DPI, 11 DPI, 12 DPI and 13 DPI using a Nikon SMZ 1500 epifluorescence stereomicroscope (n=10). These observations confirmed loss of mYFP+ objects (BPs), and the continued presence of distinctive rows of mCherry+ objects (blue-sensitive cones) within retinas at 5 DPI (data not shown). Uninjected contralateral eyes retained expression of both transgenes. In lesioned fish, new YFP+ fluorescence was observed for the first time, at 13 DPI, and so we focused our detailed analyses beginning at 13 DPI.

In addition to observing fluorescence in living adult fish, retinas were dissected and imaged as whole mounted retinas or fixed for cryosectioning. Using an antibody against PKCα, or *nyx::mYFP* transgenic fish, we were able to positively identify retinal BPs in undamaged, control retinas and in lesioned, regenerating retinas at 13, 17, and 21 DPI (Figure 3.1). Densities of *nyx::mYFP* BPs at 13 DPI and 17 DPI appeared reduced and variable, as compared to those sampled at 21 DPI, and those of undamaged, control retinas (Figure 3.1). Newly formed BPs appeared in central and peripheral retina, in all quadrants, and there did not appear to be a bias favoring a particular location of regenerated *nyx::mYFP* BPs (Figure 3.1). This time-course of BP regeneration is consistent with a protracted, asynchronous generation of new BPs, similar to that shown for HuC/D+ retinal neurons following the same type of lesion (Fimbel, Montgomery, Burket, & Hyde, 2007). Alternatively, or in addition, regenerating BPs may not show synchronous expression of the markers used to identify them.

Optically Resliced
Sections

Whole Retinas

Control

13 DPI
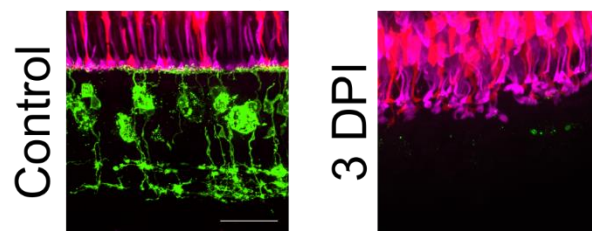
17 DPI

21 DPI
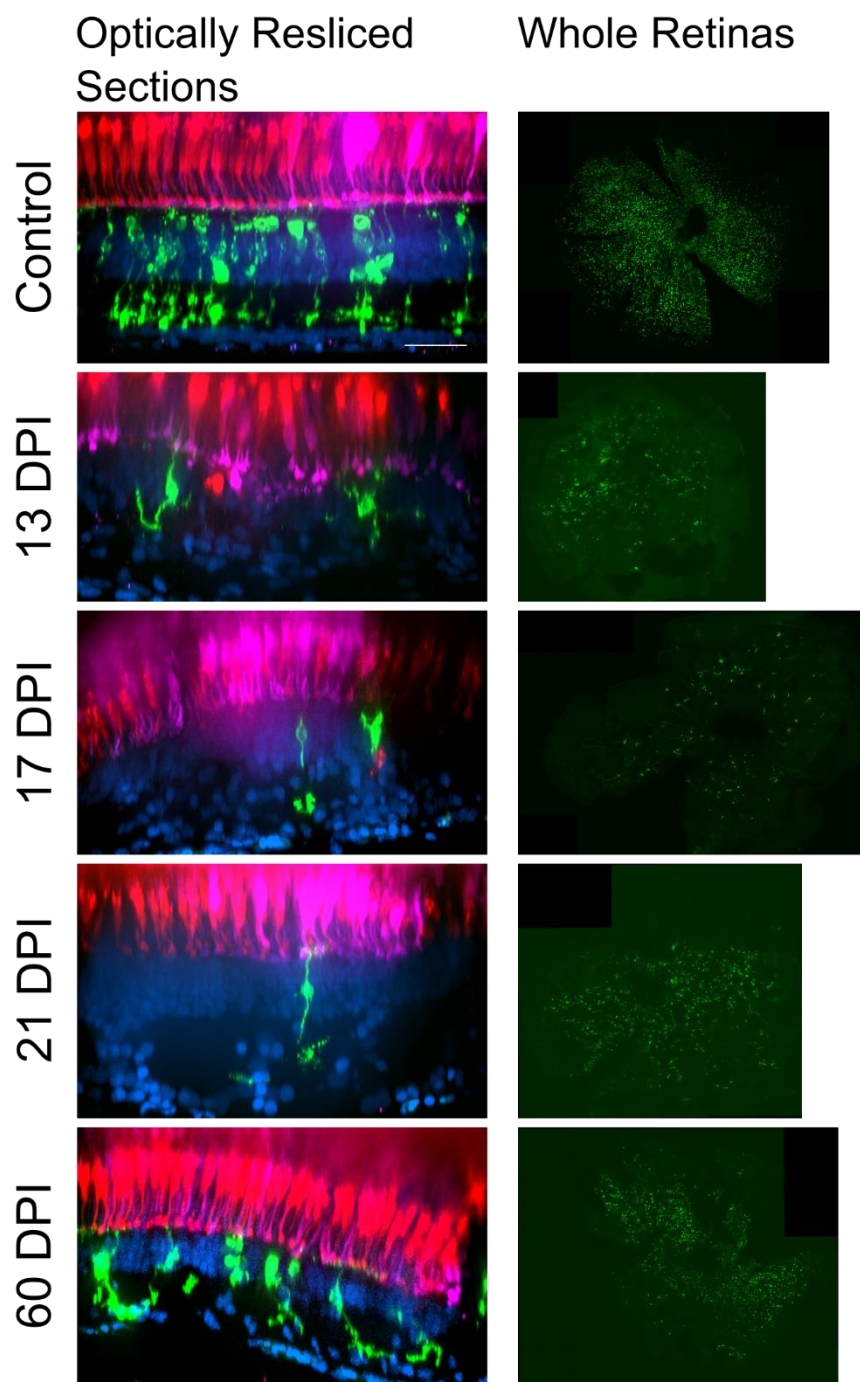
60 DPI

Cryosections

Control

3 DPI

Figure 3.1. Loss and regeneration of retinal bipolar neuron (BPs) following intravitreal injection of 2 μM ouabain. Left Column: Optical sections from control, 13 DPI, 17 DPI, 21 DPI, and 60 DPI retinas. Regions of interests (ROIs) from 60x image stacks, which were approximately 20μm wide and 160μm tall, were cropped, resliced, and projected, using max projection. By 13 DPI some of these newly form nyx::mYFP+ BPs (green) have basal and apical neurites. The SWS2:mCherry+ blue sensitive cones (red) as well as ZPR1+, double cones (magenta) appear to retain their synaptic boutons. While the overall histology of the tissue appears altered, the photoreceptor layer is still intact, but appears slightly warped compared to control retinas. Tissue at 13 DPI and 17 DPI seems more prone to this warping, which was further exaggerated as a result of flattening whole mounted retinas for microscopy (data not shown). DAPI labeled nuclei are colored blue. Right Column: *nyx::mYFP+* cells in whole mounted retinas taken at 20x and stitched together. Some nyx::mYFP+ BPs are present at 13 DPI. Scale bar=25μm

Descriptive morphologies of regenerating nyx::mYFP BPs.

Several regenerating *nyx::mYFP* BPs identified in each of (control, 13 DPI, 17 DPI, 21 DPI, respectively) whole mounted retinas sampled as controls, at 13, 17, or 21 DPI were imaged and traced (Table 3.1). Resliced Z-projections are shown in Figure 3.2, and traced, rendered neurons are shown in Figure 3.3. For purposes of comparison, a series of control, *nyx::mYFP* BPs sampled from undamaged, control retinas, is also shown in each Figure (Chapter 2). The majority of regenerating *nyx::mYFP* BPs displayed apically-projecting neurites, as well as basally-projecting neurites. For the purpose of brevity, apically-projecting neurites with terminals within or approaching the OPL will be referred to as dendrites, and basally-projecting neurites with terminals within or approaching the IPL will be referred to as axons. In general, the dendritic trees of the BPs sampled at 13 and 17 DPI appeared smaller in area, and truncated in length compared with those of BPs sampled at 21 DPI or from control retinas. In addition, at 13 and 17 DPI, not all dendritic trees projected fully into the OPL, while all of the 21 DPI BPs traced had dendritic trees that projected into the OPL (Figure 3.2). Some axons of BPs in 13 DPI retinas were apparently longer and more tortuous than those of 17 DPI, 21 DPI, or undamaged retina, and axons of 21 DPI BPs appeared to have more complex morphologies than those sampled from other regenerating or control retinas. The IPL could not be readily identified in some cases, particularly at 13 DPI, as there were many nuclei present within the regenerating IPL (Figure 3.2).

In some cases, the morphologies of regenerating BPs in 13 DPI and 17 DPI retinas were so unusual that these neurons did not have a standard bipolar cell

appearance (indicated by arrows in Figure 3.2, and shown in detail in Figure 3.4). For example, some BPs had a single major neurite that then branched into apical and basal projections (Figure 3.4), while others displayed numerous neurites projecting from the cell body (Figure 3.4). Some BPs showed highly truncated dendritic trees, visible only as short primary dendrites (Figure 3.4). In some cases, axons of regenerating BPs appeared to have elaborate branching patterns (Figure 3.4). Neurons with highly truncated dendritic trees, were excluded from the analysis of connectivity to photoreceptors.

Retina ID	Condition	Rendered	Dendritic spread	Sholl (dendrites)	Dendritic tips	Cone contacts	Sholl (axons)
1	Control		1	1			
2	Control	1	4	4			1
3	Control	3	3	3	3	3	3
4	Control		4	2			
5	Control	1	1	1	1	1	1
6	Control		2	2	1	1	1
7	Control	3	3	3	3	3	2
8	Control	1	1	1	1	1	1
9	Control	2	4	4	4	4	3
10	Control		3	3	3		
17	13 DPI	2	2	2	2	3	
18	13 DPI	2	2	2	2	2	2
19	13 DPI	1	1				
20	13 DPI		1				
21	13 DPI	6	6	6	4	2	6
22	13 DPI	2	3	3	3	3	1
24	17 DPI	3	2	2			2
25	17 DPI		3	3			1
26	17 DPI	2	1	1			1
27	17 DPI	2	2	2	2	1	1
28	17 DPI	4	4	4	4	4	3
29	21 DPI	2					
31	21 DPI		4	1			1
32	21 DPI	2	3	2	3	3	
34	21 DPI	3	3	3	2	2	3
35	21 DPI	4	3	3	2	2	1

Table 3.1. Sample Sizes. The number of neurons used for each type of measurement (Dendritic Spread, Sholl, Dendritic tips, and Cone contacts) or presented in Figure 3.3 (Rendered), from each retina is represented in each column.
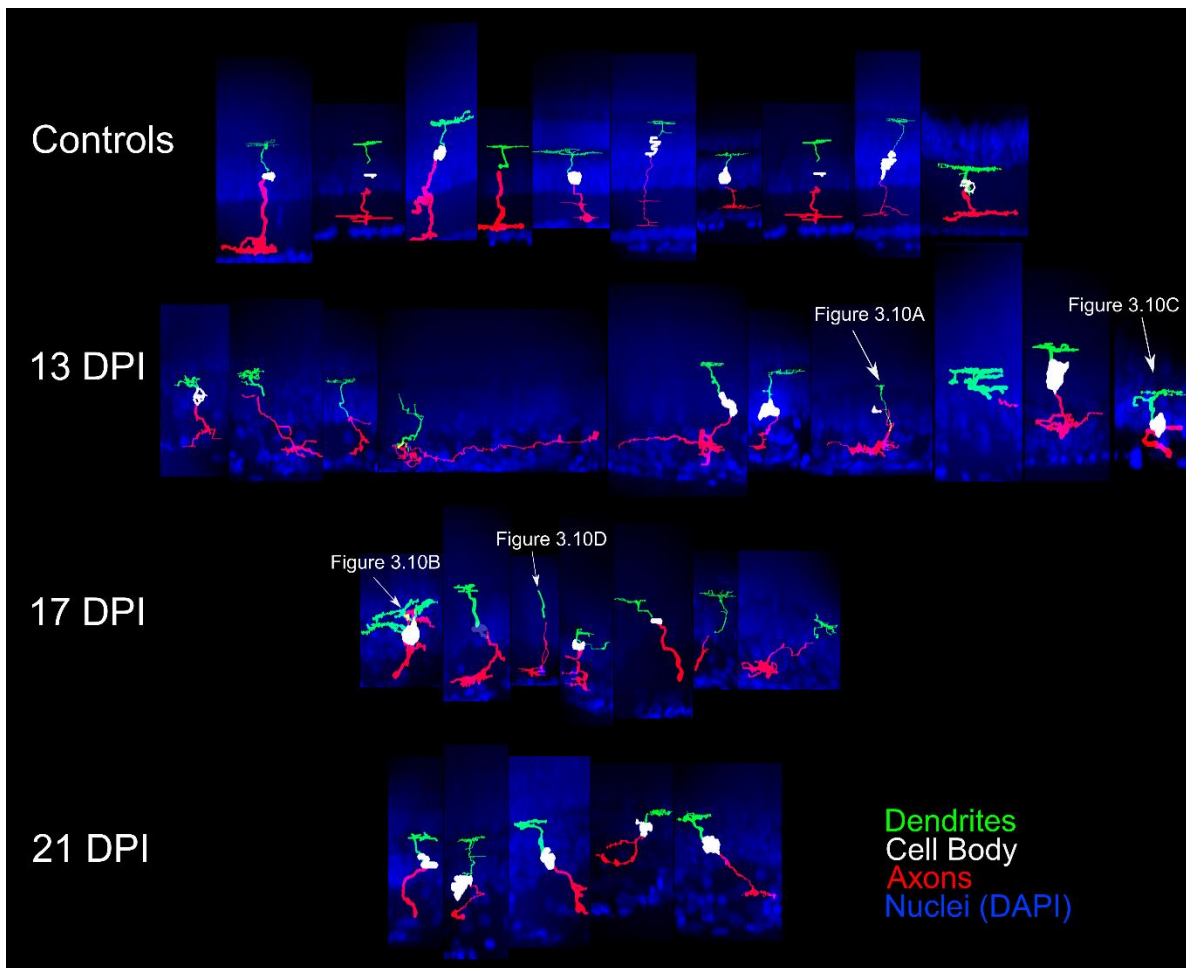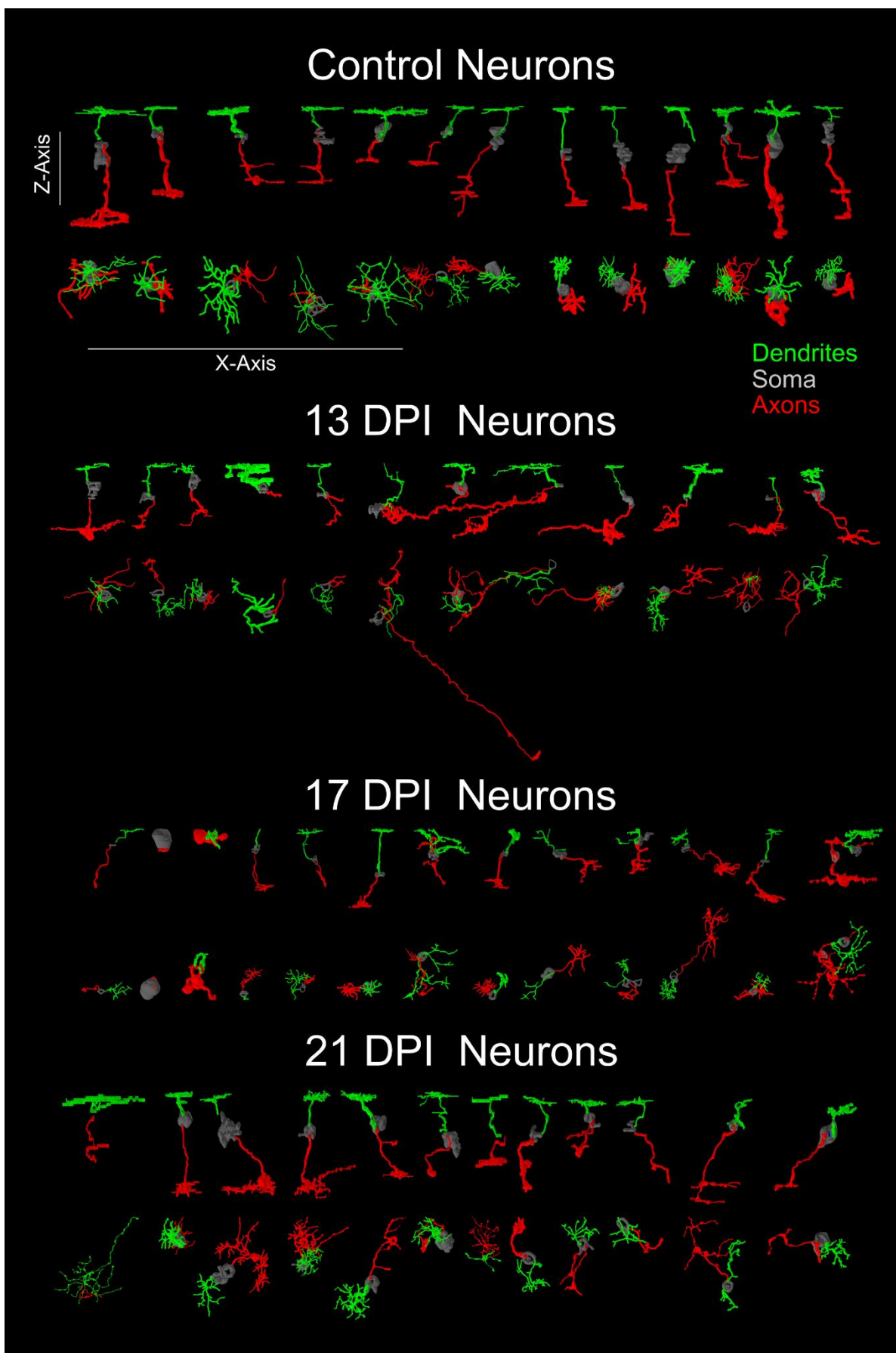
Figure 3.2. Traced *nyx::mYFP* retinal bipolar neurons sampled from control retinas (Chapter 2), and in regenerating retinas at 13, 17, and 21 days post-injury (DPI). Neurons were traced in Simple Neurite Tracer, dendrites, cell bodies, axons were colorized, and then merged with images of the nuclei that shows the retinal layers. These merged images were then resliced to show the orthogonal views and was done in a way to ensure the alignment of the traced cells and DAPI stained nuclei was preserved. Neurons at 13 DPI, 17 DPI, and to a lesser extent, 21 DPI, varied greatly in appearance. In several examples the axons would extend perpendicularly to the plexiform layers for long distances, whereas neurons from control and 60 DPI retinas tended to extend mostly from inner to outer retina, and have apparent stratifications. Other bipolar cells had extensive dendritic networks, but little to no axons or axons that more closely resembled the controls.

Control Neurons

Z-Axis

X-Axis

Dendrites
Soma
Axons

13 DPI Neurons

17 DPI Neurons

21 DPI Neurons

Figure 3.3. Renderings of traced, *nyx::mYFP* + retinal bipolar neurons (BPs) from retinas sampled from control retinas (Chapter 2), and in regenerating retinas at 13, 17, and 21 days post-injury (DPI). These neurons were traced in SNT, filled out, created into 3D surface models, imported into 3ds Max 2016, and then were placed into this one image to show overall similarities and differences of these BP cells in regenerating retinas. Presumed dendrites are colored green, cells bodies colored grey, and presumed axons are colored red.

13 DPI   17 DPI
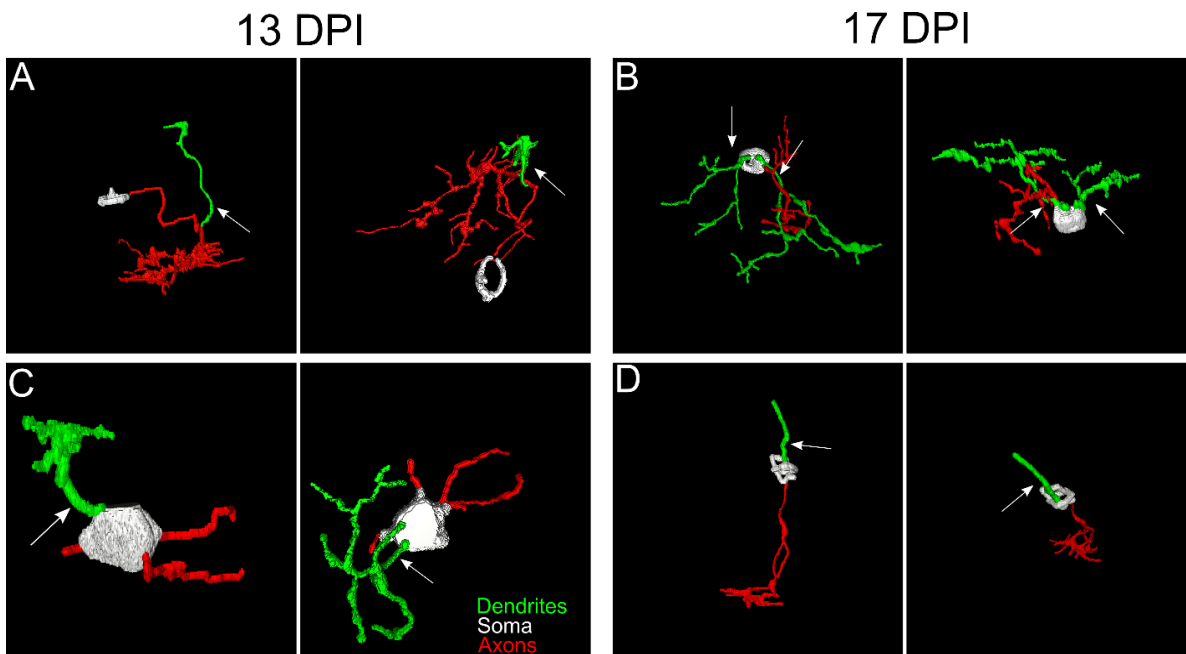
Figure 3.4. Selected retinal bipolar neurons (BPs) that demonstrate the unusual range of morphologies observed at 13 and 17 days post-injury (DPI). Neurons were traced in Simple Neurite Tracer and then rendered in ImageJ's 3D viewer. (A) Neuron that has a displaced soma and multiple neurites. (B) Neuron that has two distinct dendritic fields connected to the same cell body. (C, D) Relatively simple neurons at 13 DPI and 17 DPI respectively. In contrast to A and B, these particular cells have a bipolar shape, but have underdeveloped dendrites with fewer branches than most other neurons at that particular time point. The neuron in C appears to have an axon that is still undergoing growth and pathfinding, while the neuron in D appears to have a full or nearly full axon. Arrows designate investigator assignment of primary dendrites.

Morphometric analysis of dendritic trees of regenerating nyx::mYFP BPs.
Dendritic spread.

Measurements of dendritic field sizes were possible for 25 BPs from six control eyes, 15 BPs from six eyes sampled at 13 DPI, 13 BPs from five eyes sampled at 17 DPI, and 13 BPs from four eyes sampled at 21 DPI (Table 3.1). Interestingly, the dendritic spreads of regenerating BPs at 13 DPI were not significantly smaller than those of control BPs (p=0.216, measured by a convex polygon; p=0.072, measured by an ellipse) (Figure 3.5). However, the dendritic spreads of BPs in the 17 DPI and 21 DPI retinas were significantly smaller than those in control retinas (p=0.002 and p=0.038, complex polygon; p=0.004 and p=0.016, ellipse) (Wilcoxon–Mann–Whitney) (Figure 3.5).

Dendritic tree characteristics.

Using the Sholl Analysis plugin in ImageJ, the extent of dendritic branching was calculated separately for each individual neuron and was done by taking the sum of the number of dendrite crossings of each concentric sphere and then by dividing by the number of concentric spheres. This returned a "mean of intersections" by the plugin (Ferreira, et al., 2014). Dendritic branching was less extensive for BPs in 13 DPI retinas than for those in control retinas (p=0.006) (Figure 3.6). However, the extent of dendritic branching reached control levels for regenerating BPs sampled at 17 DPI and 21 DPI (p=0.054 and p=0.883) (Figure 3.6). Therefore, while the sizes of the dendritic trees of 13 DPI BPs were similar to those of controls, these trees were less extensively branched. Results from Sholl analysis also revealed significant reductions in the Sholl critical value for 13 DPI and 17 DPI BPs as compared with controls (p=0.0088 and p=0.0237), but dendrites of 21 DPI BPs had Sholl critical values matching those of controls (p=0.921) (Figure 3.6).

As a further measure of overall dendritic complexity, the Sholl regression coefficient was calculated, using the semi-log method (Ristanovic, Milosevic, & Stulic, 2006). A one-way ANOVA across all sampling times revealed no significant differences (p=0.444) (Figure 3.7).
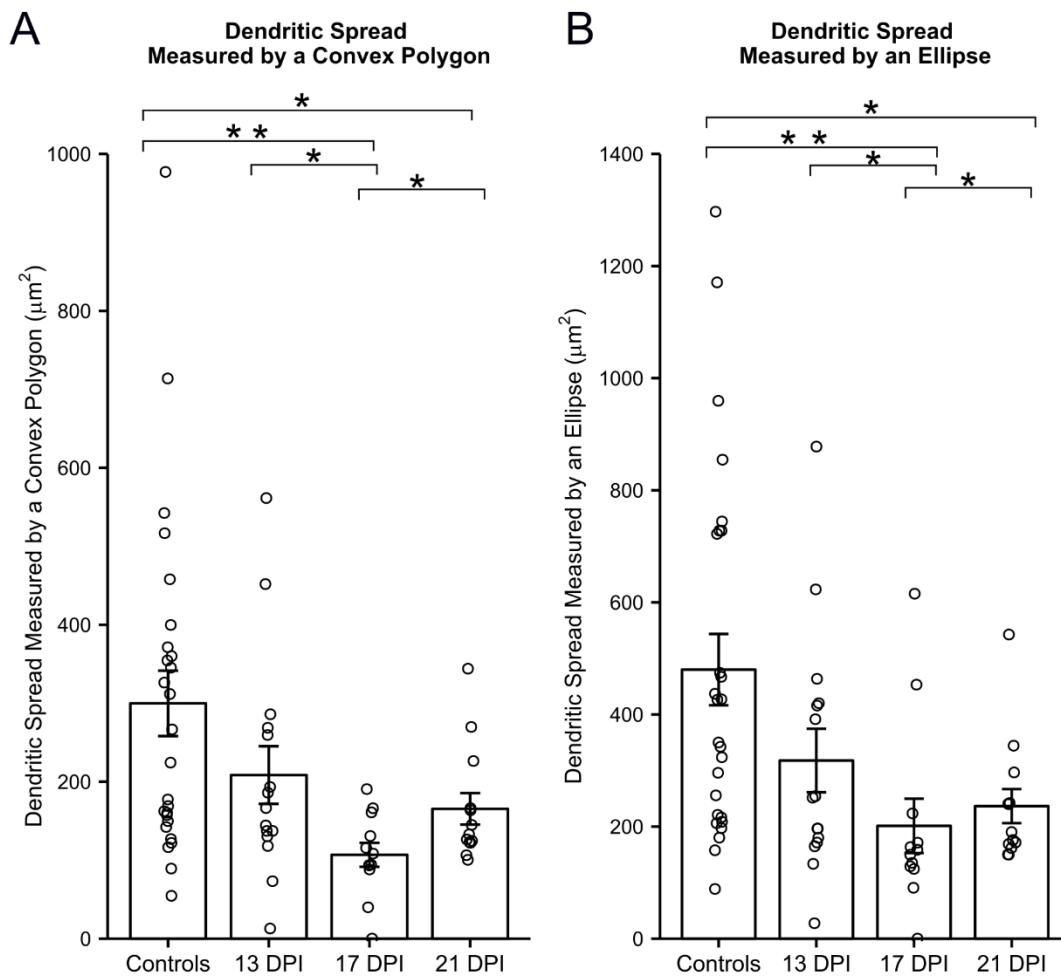
Figure 3.5. Dendritic spreads of regenerating *nyx::mYFP* bipolar neurons (BPs) are reduced at 17 and 21 DPI compared to controls. Bar graphs showing the average of each group, open circles represent each individual dendrite, and the error bars show the SEM.   *p<0.05, **p<0.01 using Wilcoxon–Mann–Whitney test.
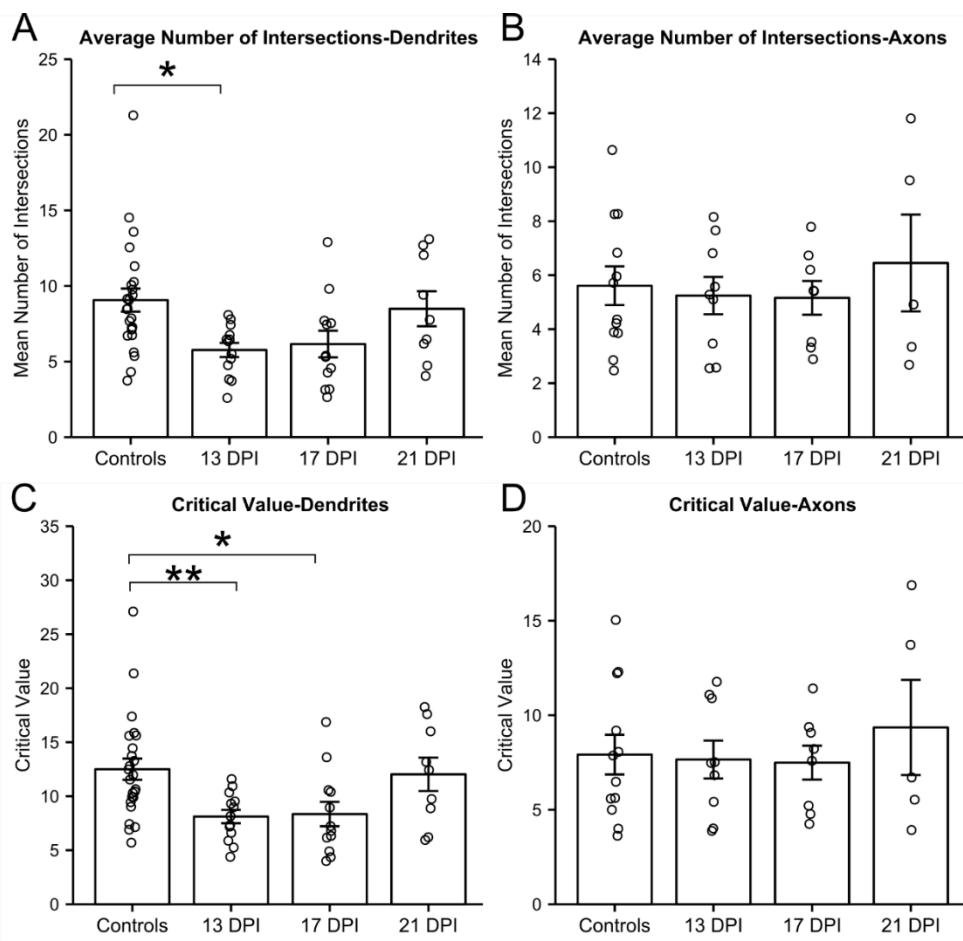
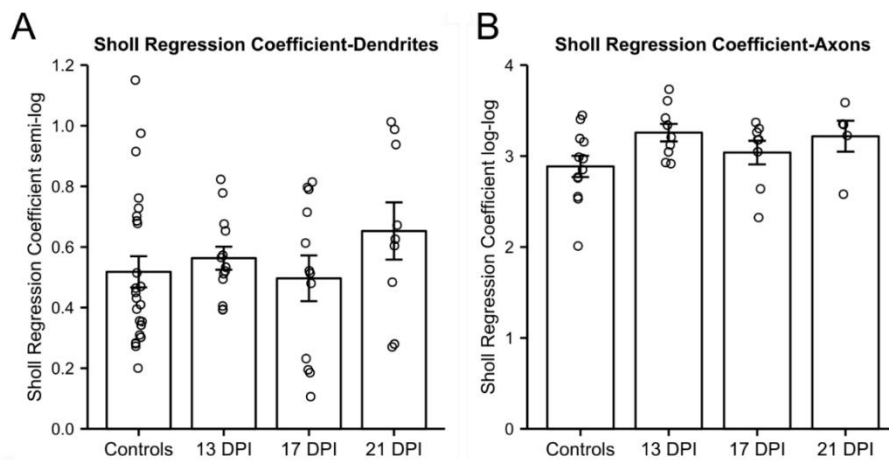Figure 3.6. Characteristics of dendritic trees and axonal branching patterns of regenerating *nyx::mYFP* bipolar neurons (BPs). Bar graphs showing the average of each group, open circles represent each individual dendrite, and the error bars show the SEM.   *p<0.05, **p<0.01 using Wilcoxon–Mann–Whitney test.

Figure 3.7. Sholl Regression. Bar graph of Sholl regression coefficients and the line graph plotting Sholl data as a linear function. (A, B) Bar graphs showing the average Sholl Regression coefficient for each time point. The values of each neuron are plotted as circles. Error bars represents the SEM.

The Average Number of Dendritic tips was no different at each time point.

Endpoints (dendritic tips) of *nyx::mYFP* BPs were counted in the three regenerating conditions, and in controls (Li, Tsujimura, Kawamura, & Dowling, 2012) (Table 3.1). The average total numbers per BP showed no statistically significant differences across all conditions (p=0.194, one-way ANOVA.) (Figure 3.8).
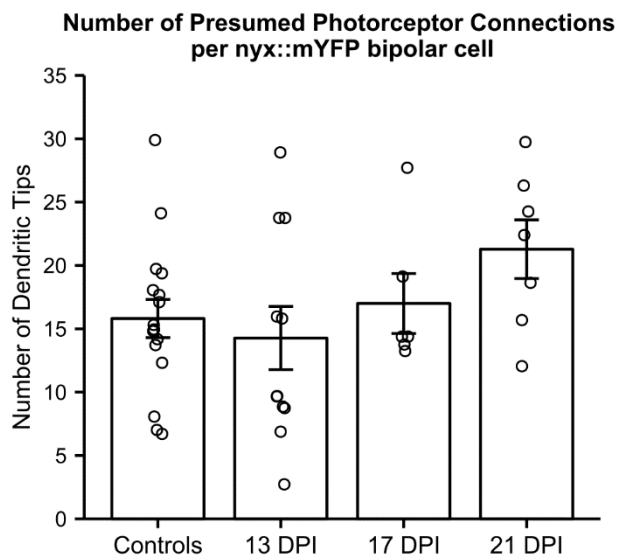

Figure 3.8. Bar graphs showing the average number of dendritic tips of time point, open circles represent each individual dendrite, and the error bars show the SEM.
Cone-bipolar connections during retinal regeneration Some bipolar cells have dendritic projections into the OPL.

Traced, *nyx::mYFP* BPs were evaluated for the presence of presumptive synaptic connections with cone photoreceptors, with mCherry+ synaptic terminals of blue-sensitive cones, and with ZPR1 stained synaptic terminals of double cones (a.k.a. red- and green-sensitive cones). For this analysis we excluded BPs that did not reach the OPL with their apical processes; these BPs are discussed in the subsequent section of Results. The patterns of connections, measured as the proportion of endpoints contacting blue cones vs. double cones vs. unassigned endpoints (UV cones, rods, or unconnected), were quantified (Figure 3.9). In Chapter 2, ZPR1+ cones could readily be identified as green sensitive or red sensitive based upon their location and surrounding cones. ZPR1+ cones in the regenerating retinas used in this study could not be easily classified as red or green

sensitive cones because they appeared to be less organized. As a result, each endpoint was counted as connecting to a blue sensitive cone, ZPR1+ cone, or unassigned. Cones from 60 DPI was reanalyzed using these criteria and included in the Generalized Linear Model.

The BPs sampled at 13, 17 DPI, and 60 DPI, each showed patterns of photoreceptor connections that were statistically indistinguishable from the controls (p=0.3844, 0.2758, and 0.4534, respectively; Generalized Linear Model) (Figure 3.9). However, the BPs sampled at 21 DPI did show a significant difference at 21 DPI (p=0.031), apparently favoring ZPR1+ double cone contacts over blue cone contacts (Figure 3.9), suggesting some plasticity of synaptic connections during regeneration.
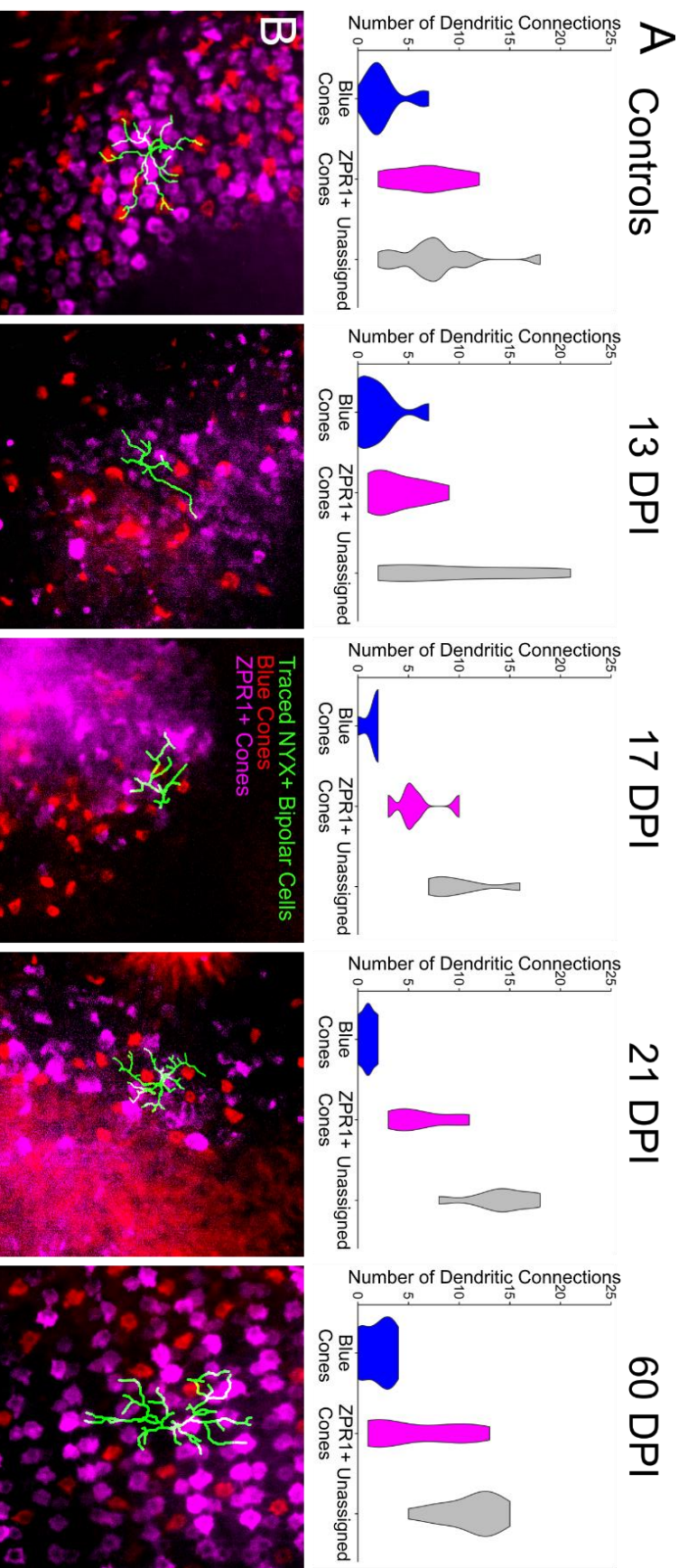
Figure 3.9. Re-establishment of BP dendritic connections with photoreceptors. A. Distributions of dendritic connections to identified and unassigned photoreceptor subtypes for *nyx::mYFP* bipolar neurons in control, 13 DPI, 17 DPI, 21 DPI, and 60 DPI retinas. Shapes of violin plots were obtained by using a kernel density estimator to generate a smoothened histogram, mirrored along the x-axis, and then rotated. The width of each plot is determined by the proportion of bipolar cells making a given number of connections to that photoreceptor subtype at that point. B. Dendritic fields showing traced NYX+ cells (green) done in Simple Neurite Tracer overlayed onto partial projections of blue sensitive (red) cones and ZPR1+ (magenta) cones. Control and 60 DPI images also appear in Chapter 2. Scale bar= 10μm

Not all bipolar cells reconnected with photoreceptors at 13 DPI and 17 DPI. Some of the neurons shown in Figure 3.3 did not appear to reach the OPL in the 13 DPI or 17 DPI groups. Two of these neurons are shown in higher detail in Figure 3.10 (these specific neurons are marked as Figure 3.10). Figure 3.10A and 3.10B shows that these dendrites terminate basally to the OPL and at most have one branch that connects with photoreceptors. Neurons with 1 or fewer projections reaching the OPL, such as those pictured in Figure 3.10 were excluded from the pattern analysis due to the ambiguity of that one connection. All of the neurons measured at 21 DPI appeared to have dendrites that projected into the OPL.

Some of the more unusual-appearing BP axons from regenerating retina were examined in further detail, and are provided as 3-D projections in order to appreciate the context of the BP axon and surrounding regenerating retinal tissue (Figures 10-14).
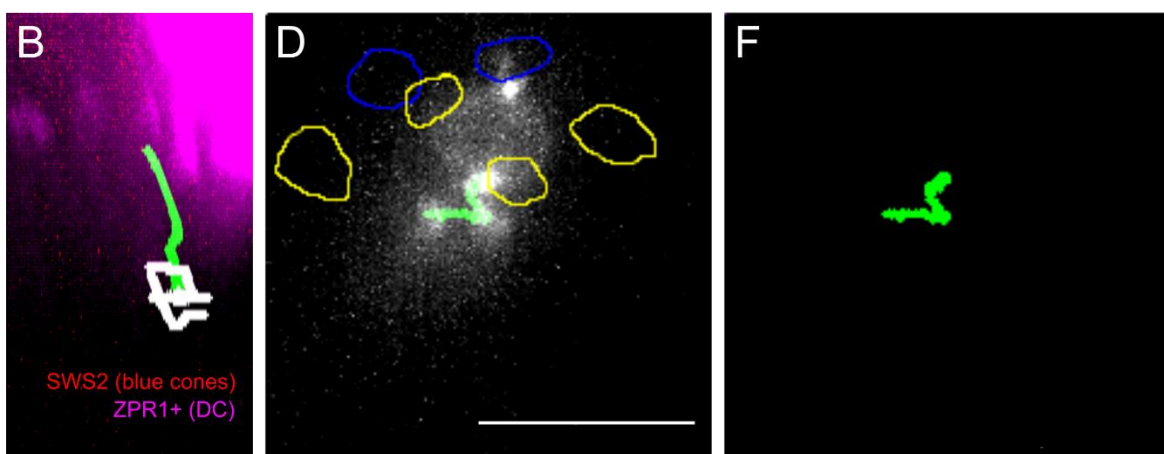
13 DPI
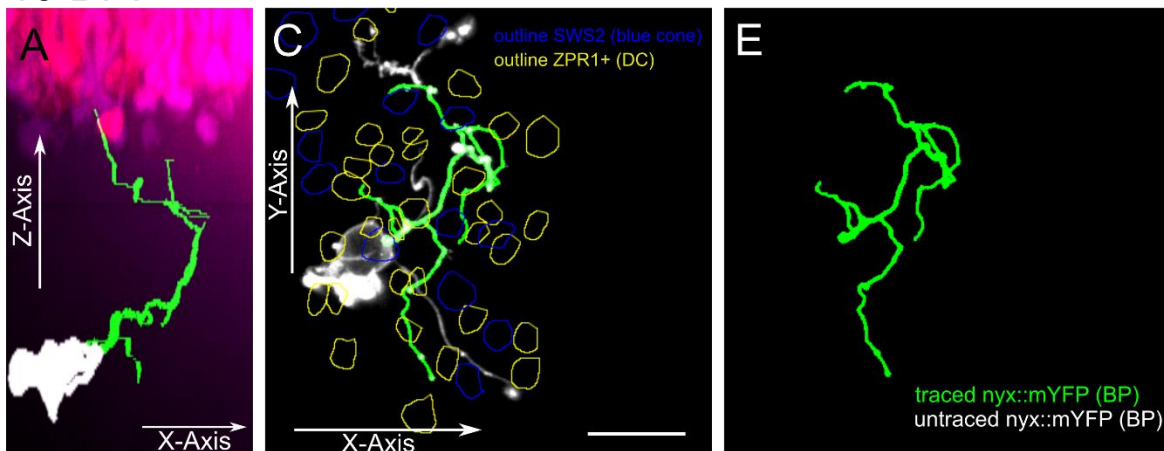
17 DPI

Figure 3.10. Not all bipolar cells have connected to photoreceptors by 13 DPI and 17 DPI. Examples of traced dendrites and somas, combined onto partially projected confocal images. Despite having a dendrite with multiple branches, none of those branches makes a presumed connection into the OPL. (A, B) Resliced view of neurons that has not yet made connections to photoreceptors. (C, D) Terminals of photoreceptors are outlined by yellow (ZPR1+ cones) and blue (blue sensitive cones). (E, F). Tracings of only the dendrites from C and D to show the morphology of these dendrites as they appear in the X-Y view. Scale bars=10μm.

Discussion

We report neuronal morphologies and cone connectivities of regenerating BPs in adult retina over the time of emergence of retinal plexiform layers. After a 2 μM ouabain-induced lesion of all inner retinal neurons (Raymond, Reifler, & Rivlin, 1988), (Fimbel, Montgomery, Burket, & Hyde, 2007), (Sherpa, et al., 2014), and (Chapter 2), regenerating BPs must establish morphologies that allow them to ultimately carry out their specific functions and communicate with appropriate synaptic partners. They

must find their inputs (photoreceptors, which were not damaged by the lesion) (Fimbel, Montgomery, Burket, & Hyde, 2007), and their outputs (amacrine and ganglion cells, which must regenerate following the lesion). We find that new, *nyx::mYFP*+ BPs are apparent in regenerating retinas at 13, 17, and 21 DPI, but in smaller numbers than control or 60 DPI retinas (Chapter 2) This is consistent with protracted and asynchronous regeneration or expression of BP markers. The morphologies of *nyx::mYFP*+ BPs sampled at 13, 17, and 21 DPI were in some cases highly unusual, with abnormal positions and sizes of apically and basally-projecting neurites, and/or laterally projecting axons, and/or no cone contacts. Other BPs were more stereotypical in appearance, resembling those of undamaged retinas. Dendritic tree sizes were reduced as compared with controls at 17 and 21 DPI although not at 13 DPI, while Sholl analysis indicated reduced dendritic complexity at 13 DPI. In contrast with the strikingly normal morphologies of *nyx::mYFP*+ BPs at 60 DPI (Chapter 2), the findings of the current study suggest that from 13-21 DPI, regenerating BPs are likely in the process of establishing their mature morphologies.

It is notable, however, that the average total of dendritic tips did not significantly vary. The distribution of cone contacts (where present) by cone type was not significantly different at 13, 17, and 60 DPI, with only minor differences at 21 DPI. This suggests minimal BP-photoreceptor synaptic plasticity during regeneration. Another possibility is that BPs that have not made connections to photoreceptors at 13 and 17 DPI, reconnect by 21 DPI, but their resulting connectivity pattern is different from those bipolar cells that made connections prior to 13 DPI.

Some bipolar cells restore apparent cone contacts by 13 DPI.

Although not all BPs showed visible connections to photoreceptors at 13 DPI and 17 DPI (Figure 3.10), those that did, showed cone connectivities matching those of control BPs. Interestingly, dendritic tree attributes of the regenerating BPs did show some statistically significant differences from controls (discussed in the next section). We hypothesize based upon these findings that BPs make their connections to photoreceptors before their dendritic trees are mature (Figure 3.10). Additional research is needed to determine whether the apparent cone-BP connections

observed at 13, 17, and 21 DPI are permanent. Alternatively, instead of undergoing morphological changes later in regeneration, some of these regenerated BPs might undergo apoptosis while new BPs continue to be generated and assume normal morphologies and connectivities. This alternative explanation seems unlikely for several reasons. TUNEL labeling for apoptotic retinal neurons indicates that a large scale die-off of cells does not take place after the initial (3-5 DPI) period of cell death due to ouabain damage (Fimbel, Montgomery, Burket, & Hyde, 2007). Additionally, Hitchcock & Cirenza (1994) found that amacrine cells were able to remodel and reintegrate into regenerated portions of the retina following surgical excision. It would be surprising if bipolar cells lacked the same ability as amacrine cells to remodel or change their morphology.

Attributes of dendritic tree morphologies vary during the regeneration of retinal BPs..

Critical values of the 13 DPI and 17 DPI, but not the 21 DPI, BP dendritic trees, were different from the controls. This suggests that new dendritic branches are formed around 13 DPI but still continue to form and grow until 21 DPI. This does not exclude the possibility that dendritic outgrowth and dendritic pruning might continue even after 21 DPI, but would do so at a steady state.

In contrast, the mean number of intersections was reduced for BP dendrites at 13 DPI, but not for those sampled at 17 DPI or 21 DPI. Even though this type of measurement is not equivalent to directly counting the number of branches for each neuron, these results still provide evidence that regenerating *nyx::mYFP* BPs sampled at 13 DPI have dendritic trees with fewer branches, shorter branches, or a combination of both, as compared with other sampling conditions. In general, the outputs of Sholl analysis indicate that the dendritic trees of sampled, regenerating BPs are likely undergoing morphological changes over the 13-21 DPI sampling time.

Finally, dendritic field sizes of regenerating BPs were reduced at 17 and 21 DPI as compared to controls. Results from Chapter 2 showed that dendritic field size, mean number of intersections, and critical values of dendrites of regenerated *nyx::mYBP* BPs were all restored by 60 DPI. Together with the results from the current study, this indicates that BP development, growth or generation continues in a regenerating retina between 21 DPI and 60 DPI.
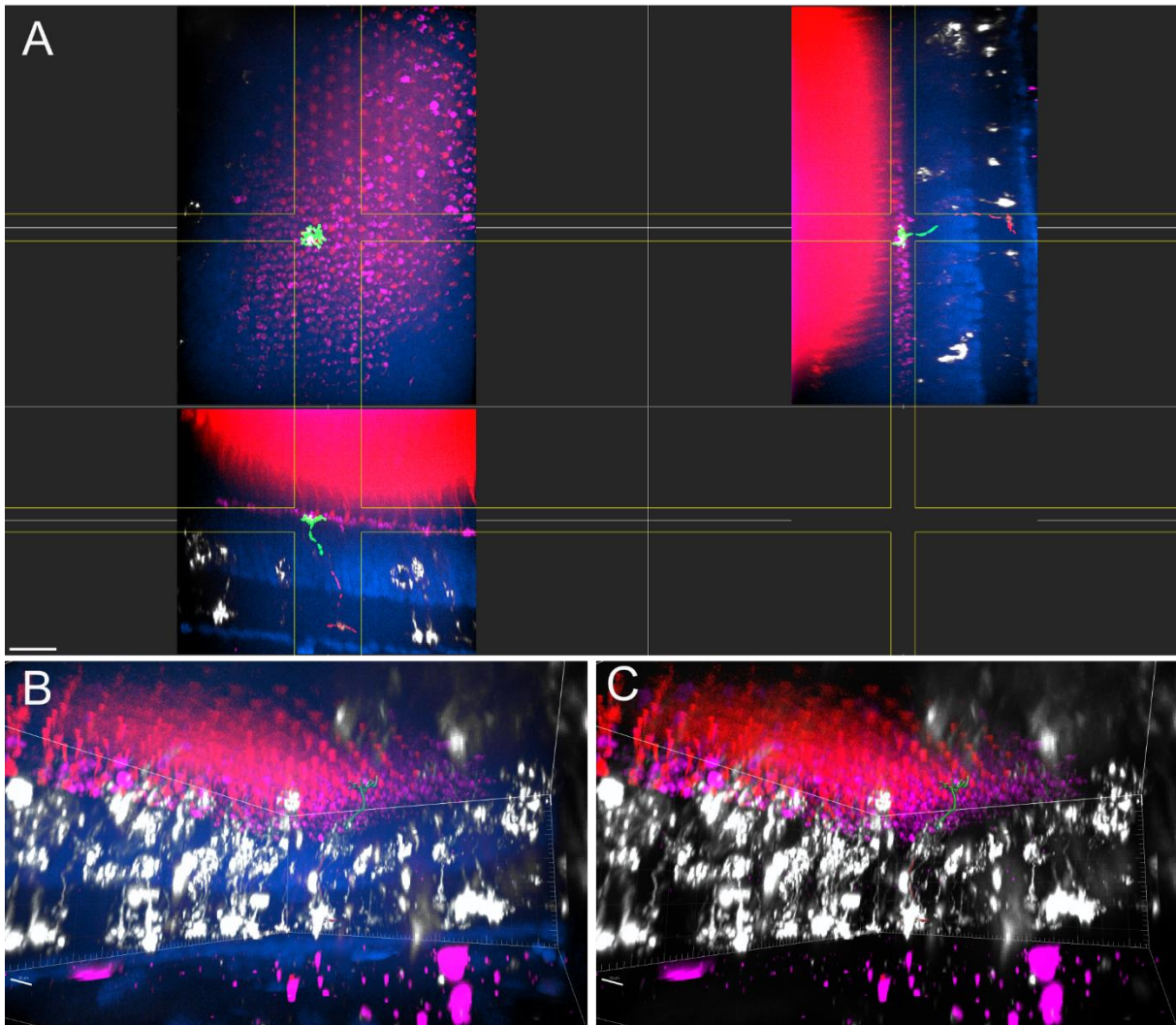
Control

Figure 3.11. Pictures and tracings of a neuron within a control retina. (A) Dendrite and axon was traced by the filament tracer plugin in Imaris, and converted into a green or red color channel respectively. All color channels were projected as a maximum intensity projection to visualize *nyx::mYFP* neurons (grayscale), blue sensitive photoreceptors (red), ZPR1+ cone photoreceptors (magenta) and DAPI stained nuclei (blue), traced dendrite (green), and traced axon (red). The yellow cross hairs show the thickness of the adjacent images, indicating how much of the retina is projected. (B,C) Perspective view of the same neuron showing how the neuron is positioned and integrated into the retinal landscape. The traced axon is colored red while the traced dendrite is colored green. Untraced neighboring *nyx::mYFP* + neurons are colored in grayscale. SWS2:mCherry+ blue sensitive photoreceptors are colored red, while ZPR1+ photoreceptors are magenta. Nuclei stained by DAPI are colored blue (A,B).
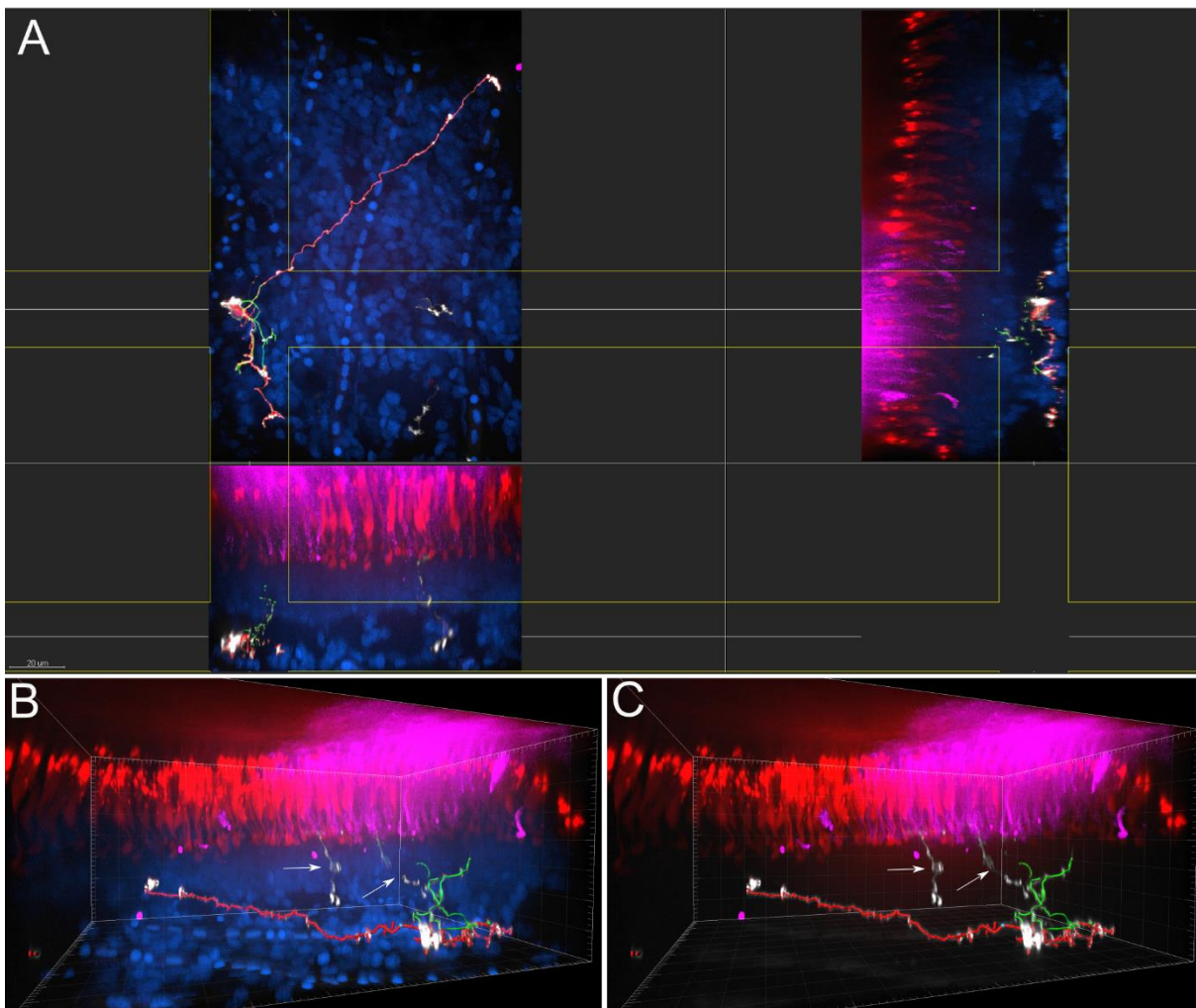
13 DPI

Figure 3.12. Pictures and tracings of a neuron within a 13 DPI retina. (A) Dendrite and axon was traced by the filament tracer plugin in Imaris, and converted into a green or red color channel respectively. All color channels were projected as a maximum intensity projection to visualize *nyx::mYFP* neurons (grayscale), blue sensitive photoreceptors (red), ZPR1+ cone photoreceptors (magenta) and DAPI stained nuclei (blue), traced dendrite (green), and traced axon (red). The yellow cross hairs show the thickness of the adjacent images, indicating how much of the retina is projected. (B,C) Perspective view of the same neuron showing how the neuron is positioned and integrated into the retinal landscape. The traced axon is colored red while the traced dendrite is colored green. Arrows indicate neighboring, untraced *nyx::mYFP* + neurons (grayscale). SWS2:mCherry+ blue sensitive photoreceptors are colored red, while ZPR1+ photoreceptors are magenta. Nuclei stained by DAPI are colored blue (A,B).
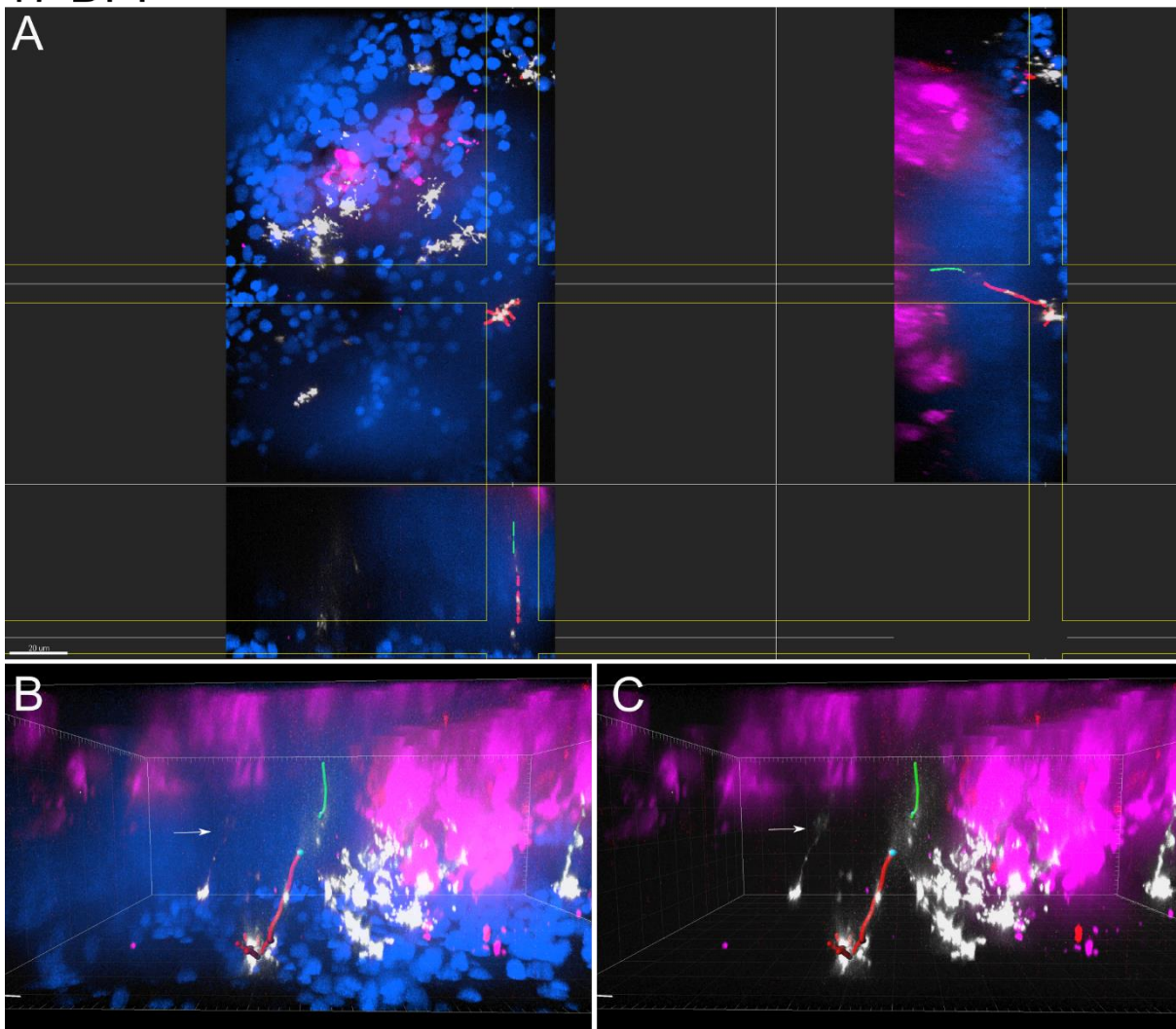
17 DPI

Figure 3.13.   Pictures and tracings of a neuron within a 17 DPI retina. (A) Dendrite and axon was traced by the filament tracer plugin in Imaris, and converted into a green or red color channel respectively. All color channels were projected as a maximum intensity projection to visualize *nyx::mYFP* neurons (grayscale), blue sensitive photoreceptors (red), ZPR1+ cone photoreceptors (magenta) and DAPI stained nuclei (blue), traced dendrite (green), and traced axon (red). The yellow cross hairs show the thickness of the adjacent images, indicating how much of the retina is projected. (B,C) Perspective view of the same neuron showing how the neuron is positioned and integrated into the retinal landscape. The traced axon is colored red while the traced dendrite is colored green. Arrows indicate neighboring, untraced *nyx::mYFP* + neurons (grayscale). SWS2:mCherry+ blue sensitive photoreceptors are colored red, while ZPR1+ photoreceptors are magenta. Nuclei stained by DAPI are colored blue (A,B).
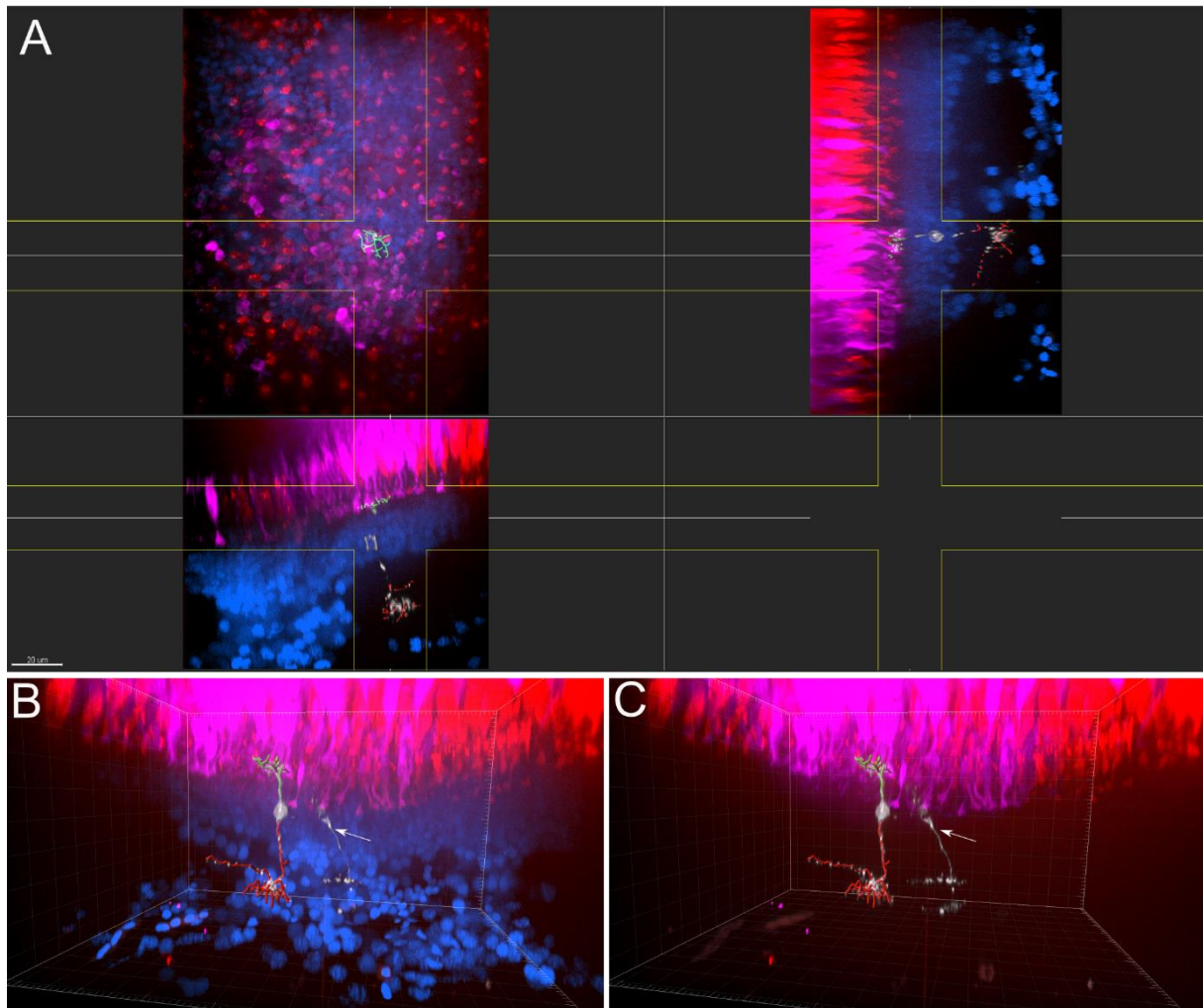
21 DPI

Figure 3.14.   Pictures and tracings of a neuron within a 21 DPI retina. (A) Dendrite and axon was traced by the filament tracer plugin in Imaris, and converted into a green or red color channel respectively. All color channels were projected as a maximum intensity projection to visualize *nyx::mYFP* neurons (grayscale), blue sensitive photoreceptors (red), ZPR1+ cone photoreceptors (magenta) and DAPI stained nuclei (blue), traced dendrite (green), and traced axon (red). The yellow cross hairs show the thickness of the adjacent images, indicating how much of the retina is projected. (B,C) Perspective view of the same neuron showing how the neuron is positioned and integrated into the retinal landscape. The traced axon is colored red while the traced dendrite is colored green. Arrows indicate neighboring, untraced *nyx::mYFP* + neurons (grayscale). SWS2:mCherry+ blue sensitive photoreceptors are colored red, while ZPR1+ photoreceptors are magenta. Nuclei stained by DAPI are colored blue (A,B).

References

Ferreira, T. A., Blackman, A. V., Oyrer, J., Jayabal, S., Chung, A. J., Watt, A. J., . . . van Meyel, D. J. (2014, October 11). *Neuronal Morphometry Directly from Bitmap Images.* Nature Methods, 11(10), 982-984.

Fimbel, S. M., Montgomery, J. E., Burket, C. T., & Hyde, D. R. (2007, February 14). *Regeneration of Inner Retinal Neurons after Intravitreal Injection of Ouabain in Zebrafish.* The Journal of Neuroscience, 27(7), 1712-1724.

Hitchcock, P. F., & Cirenza, P. (1994, May 22). *Synaptic Organization of Regenerated Retina in the Goldfish.* Journal of Comparative Neurology, 343(4), 609-616.

Raymond, P. A., Reifler, M. J., & Rivlin, P. K. (1988, July). *Regeneration of goldfish retina: rod precursors are a likely source of regenerated cells.* Journal of Neurobiology, 19(5), 431-463.

Ristanovic, D., Milosevic, N., & Stulic, V. (2006, December 15). *Application of modified Sholl analysis to neuronal dendritic arborization of the cat spinal cord.* Journal of Neuroscience Methods, 158(2), 212-218.

Schroeter, E. H., Wong, R. O., & Gregg, R. G. (2006, September-October). *In vivo development of retinal ON-bipolar cell axonal terminals visualized in nyx::MYFP transgenic zebrafish.* Visual Neuroscience, 23(5), 833-843.

Sherpa, T., Lankford, T., McGinn, T. E., Hunter, S. S., Frey, R. A., Ryan, M., . . . Stenkamp, D. L. (2014, September 1). *Retinal Regeneration is Facilitated by the Presence of Surviving Neurons.* Developmental Neurobiology, 74(9), 851-876.

Sholl, D. A. (1953, October). Dendritic Organization in the Neurons of the Visual and Motor Cortices of the Cat. Journal of Anatomy, 87(4), 387-406.

Takechi, M., Hamaoka, T., & Shoji, K. (2003, October 9). *Fluorescence visualization of ultraviolet-sensitive cone photoreceptor development in living zebrafish.* FEBS Letters, 553(1-2), 90-94.

Takechi, M., Seno, S., & Kawamura, S. (2008, November 14*). Identification of cis-Acting Elements Repressing Blue Opsin Expression in Zebrafish UV Cones and Pineal Cells.* J. Biol. Chem., 31625-31632.

Westerfield M (2007) The Zebrafish Book; A guide for the laboratory use of zebrafish (Danio rerio). Eugene, OR: University of Oregon Press.